PHYSICAL REVIEW A VOLUME 25, NUMBER 1 JANUARY 1982

Excitation of the helium autoionizing states in $He^+ + He$ collisions, between 3 and 140 keV

A. Bordenave-Montesquieu, A. Gleizes, and P. Benoit-Cattin

Centre de Physique Atomique, Equipe de Recherche Associée au Centre National de la Recherche Scientifique n °598, Université Paul Sabatier, 118, Route de Narbonne, 31062 Toulouse Cedex, France

(Received 22 October 1980)

The autoionization of the helium atom has been experimentally studied in $He^+ + He$ collisions between 3 and 140 keV by electron spectrometry. The excitation of the two collision partners has been considered. Above 10 keV, the shapes and excitation cross sections of the $2s^2\,{}^1S$, $2s2p\,{}^3P$, $2p^2\,{}^1D$, and $2s2p\,{}^1P$ are determined by a numerical fitting procedure which is reported in detail; below 10 keV the $({}^1D + {}^1P)$, and $2p^2\,{}^1S$ line intensities are obtained by planimetry since important post-collision effects are observed. From the angular distributions measured below 15 keV, the relative sublevel populations are deduced for the $2p^2\,{}^1D$ and $2s2p\,{}^1P$ levels and are compared with those obtained by other authors in a coincidence experiment; the excitation processes are then discussed within the quasimolecular-excitation model. For the highest collision energies, the asymmetry of the angular distributions with respect to 90° as well as the line shapes above 100 keV are interpreted by the occurrence of sudden electronic transitions to the continuum. A comparison of the differential cross sections for emission of electrons by autoionization of the fast and slow particles permits us to show that the quasimolecule model cannot explain what is observed above a collision velocity of about 0.5 a.u. The dependence of the total cross sections against the collision energy is also discussed in terms of an evolution of the excitation mechanism from a quasimolecular to an atomic one; the specific variation of the $2s2p\,{}^3P$ cross section strengthens this interpretation. These total cross sections are compared with those estimated from earlier $H^+ + He$ data published by us; similar autoionization cross-section values are expected for the two systems at high collision velocity.

I. INTRODUCTION

Ionization processes in the neighborhood of the autoionizing states, in the energy range extending above a few tens of keV for light atoms, are well described by an atomic mechanism where two competing processes populate the continuum: a direct ionizing transition and an indirect one through the excitation of an autoionizing level. This is the well-known phenomenon described by Fano[1] for the inelastic scattering processes and by Balashov and co-workers for the ejection of electrons.[2] In the latter case, interference between these two transition amplitudes can induce asymmetrical line shapes in the ejected electron spectra in the vicinity of the energetic positions of the autoionizing states and also asymmetrical angular distributions of these lines. The former phenomenon was first observed in collisions between heavy partners for the H^+-He system[3,4] which was intensively studied[5-8]; in the energy range where the Born approximation applies, a theoretical investigation was also made.[9] For more complex systems, only fragmentary experimental results appear for He^+ and He^{2+} on He systems[10] but no theoretical study exists. As shown by Balashov[2] the analysis of the autoionizing lines in the ejected electron spectra using Shore's or Fano's formulas can be made at the expense of a loss of a clear physical meaning of Shore's or Fano's parameters. This is particularly true for the Shore parameter b which describes the line area; its theoretical expression[2,11] contains interference terms between the resonant and all the nonresonant partial waves of the continuum and generally angular distributions asymmetrical with respect to 90° must be observed. This was verified by Schowengerdt and Rudd[12] in H_2^+-He and by our group for the H^+-He collisional system.[7,8]

A symmetrical distribution is only recovered when interference terms in b are small, which can occur in the important case where the direct ionizing transition amplitude becomes small with respect to the autoionizing one. Therefore, the angular distribution only depends on the angular momentum of the autoionizing state and the theory of Cleff and Mehlhorn[13] can be applied.[14] This especially occurs when the relative velocity of the two collision partners becomes so low with respect to the orbital velocity of the atomic electrons that quasimolecular mechanisms can take place. We have already shown[14,15] that the observations are in good agreement with the quasimolecule model for the lowest energies studied in this work. For example, in He^+-He collisions at 15 keV, we have verified that the shape of the angular distribution is determined by the angular momentum of the excited state alone. This means that interference effects, such as those observed in $H^+ + He$ collisions, do not have a noticeable influence on the single differential cross sections (SDCS); indeed, this is in agreement with a pure molecular mechanism where only indirect ionizing transitions, through electron promotion and autoionization of the excited molecular state, happen. At higher energies direct transitions to the continuum

may occur, even in a quasimolecular framework, through a direct coupling of the entrance channel, or may be of a singly excited exit channel coupled to it at small internuclear distance, to the continuum. In this case, the same interference effects as those observed in atomic processes would be possible which would indicate a departure from a pure molecular mechanism.

In the energy range where the molecular model applies, autoionization of the atom occurs in the Coulomb field of the ion. Perturbations of the electron energy distributions are then observed which are more or less pronounced depending on the collision velocity. They are known as "post-collision-interaction" (PCI) effects. In He^++He collisions, at 1.4 keV collision energy, Morgenstern *et al.*[16] have shown that complex structures observed in the electron energy spectra result from interference between autoionization transition amplitudes at various internuclear distances R issued from the molecular states correlated at infinite R to the $2s^2\,{}^1S$, $2p^2\,{}^1D$, and $2s2p\,{}^1P$ atomic states. The same phenomena have also been observed by us between 3 and 10 keV (an example is given at 7 keV in Fig. 1 of Gleizes *et al.*[17]). These PCI perturbations are less and less important as the collision energy increases so that we have neglected them in our numerical analysis of the electron line shapes above 10 keV. Without allowance for interference between autoionizing transition amplitudes, the line shape is described by Barker and Berry's formula,[18] which is called the Berry effect (in Gleizes *et al.*,[19] the same phenomena was named "Stark effect" following other authors).

As shown by Stolterfoht *et al.*,[20] the Coulomb field of the ion may also perturb the excited atom by a true Stark effect. This may give rise to new structures in the neighborhood of the $2p^2\,{}^1D$ and $2s2p\,{}^1P$ line positions due to an energetic splitting of the mixed Stark states which increases with decreasing internuclear distance.[21] In our work, no clear evidence for this effect has been observed. It must be noticed that PCI interference between the ^1D and ^1P transition amplitudes and Stark mixing of the substates happen simultaneously so that both effects would have to be taken into account; however, at that time, no unified theoretical description of the whole effect of the Coulomb field on the autoionization exists and we have not considered further the Stark effect.

In this paper, we give detailed experimental results of a systematic inquiry we have done of the energy range 3 to 140 keV, in order to attempt to observe an evolution of the excitation mechanisms. The electrons ejected by autoionization of the helium states $2s^2\,{}^1S$, $2s2p\,{}^3P$, $2p^2\,{}^1D$, $2s2p\,{}^1P$, and $2p^2\,{}^1S$ excited in He^++He collisions are detected and various parameters are measured.

The line shape. In the energy range investigated in this paper, a line shape evolution was observed when the collision energy increases from 3 keV (PCI shapes) to 140 keV (Fano profiles) as shown in Sec. III C.

The angular distributions also give useful indications because PCI interferences, Stark mixing, as well as Fano interferences, may destroy the dependence of the angular distribution against the electron angular momentum. On the other hand, if this distribution is not perturbed, i.e., if it is symmetrical with respect to 90° emission angle with the correct angular momentum dependence, the sublevel populations of the autoionizing state involved may be extracted as first shown in a previous letter.[14] From them, we may infer the molecular mechanisms which lead to the atomic state excitation.

The comparison of the slow- and fast-particles autoionization cross sections may be a supplementary test. At low energy, where a quasimolecular model correctly describe the collision mechanisms, the He^++He system is symmetrical and the same doubly differential cross sections (DDCS), SDCS, and total cross sections are expected as first explained in a letter.[17] On the contrary, at much higher energy, within an atomic excitation model, it may be surmised that the direct excitation cross section of the target differs from the excitation cross section through charge exchange of the incident ion. Thus, discrepancies between the two cross sections indicate departure from a molecular model. Comparison of these cross sections makes necessary a careful analysis of the kinematic corrections to be applied to the measured values since it can only be made in an atomic emitter frame defined in the center-of-mass (c.m.) system[17]; this will be discussed in Sec. IV B.

Total cross sections, obtained by integration of SDCS over the emission angle, are determined for each autoionizing level. From their variation with the collision energy, the influence of the quasimolecular excitation mechanisms may also be observed (Secs. V and VI). Finally we compare the total cross sections obtained for H^++He and He^++He collisional systems (Sec. VII). Other work on He^++He collisions with a similar purpose was not previously reported in the literature.

II. EXPERIMENTAL METHOD

A. The experimental apparatus

A detailed description of the apparatus has been given elsewhere.[22] A mass analyzed ion beam with

a 2-mm diameter impinges on a static helium target gas. The ion-beam intensity is measured on a plane copper collector C (Fig. 1) at ground potential which is inclined at 45° relative to the incident beam direction; it is surrounded by a cylinder biased to prevent any secondary electron to escape from the collector. At the entrance of the collector a diaphragm D_1, electrically connected to the ground potential prevents stray electrical fields from penetrating in the collision chamber; it cannot intercept the incident beam.

The acceptance angle of the electrostatic analyzer as defined by the analyzer rectangular entrance slit S_0 and another circular diaphragm D_2 (1.92 ± 0.02-mm diameter) placed in front of it, varies from ±1.3° when $S_0 = 0.44 \pm 0.01$ mm [analyzer resolution full width at half maximum (FWHM) = 1.1%] to ±1.2° with $S_0 = 0.27 \pm 0.01$ mm (FWHM = 0.67%) in the horizontal plane and is equal to ±1.4° in the vertical plane. The effective solid angle of this system varies from 1.09×10^{-4} to 0.67×10^{-4} sr depending on the slit width. Most of our more recent results have been obtained with the greatest resolution.

The electrons are detected on a channeltron electron multiplier (CEM) Mullard B419 BL with a 10-mm entrance diameter biased to +300 V to accelerate the electrons at the analyzer exit in order to have a good efficiency. The stray magnetic fields are reduced in the collision chamber to a value generally lower than 5 mG by three mutually perpendicular sets of 2.2-meters-square Helmholtz coils. The target gas pressure in the collision chamber is measured with a triode ionization gauge calibrated against a liquid N_2 trapped McLeod gauge. For the results reported here we used a cyclic sweeping where a step voltage ramp was simultaneous applied to the analyzer and to the multichannel; the accumulation time in each channel is controlled by an ion charge integrator.

To be sure that a partial neutralization of the ion beam does not give important errors in our measurements (excitation of the autoionizing states by neutral particles), only very low pressures, from 5×10^{-5} to 1×10^{-4} torr for 10–140-keV He^+ energy, have been used. Therefore it was not necessary to apply any absorption correction to our cross sections. Absolute values of the cross sections were not directly obtained because the analyzer transmission t_a and the detector efficiency η remained unknown. The product (ηt_a) was obtained by normalization of our DDCS measured in $H^+ + He$ collisions to those of Rudd *et al.*[23,24] as already reported in another paper.[7] (The values of the cross sections obtained by Rudd *et al.*[23,26] have been recently tabulated by Rudd *et al.*[24] but the previous value used to normalize our results[7] still is correct and has been kept for the present normalization.) The normalization point corresponds to electrons of 33 eV kinetic energy (below the

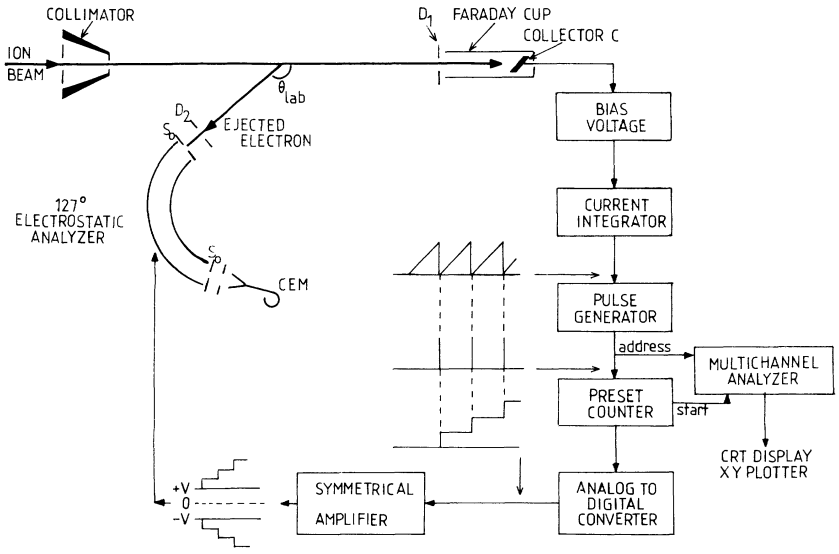

FIG. 1. Schematic diagram of the apparatus.

$2s^2\,{}^1S$ resonance) ejected by 150 keV protons at 20°; the value used is $(3.0 \pm 0.6)\ 10^{-23}\ m^2\,eV^{-1}\,sr^{-1}$ for this direct ionization DDCS; the error of ±20% is that given recently by Rudd *et al.*[24] To test this normalization, a comparison of our normalized[25] $H^+ + He$ DDCS with more recent values of the same authors[23,26] has been made. An overall agreement within ±10% is obtained below 90° and within ±30% for the great ejection angles; this precludes any systematic error in the measurement of the cross sections given in this paper.

It is worth mentioning that the use of a CEM Mullard B419 BL may be a source of systematic error in the cross section measurement. As shown by Slevin *et al.*,[27] this CEM does not have a correct characteristic curve since if we plot the measured counts against the applied voltage we do not observe a plateau as might be expected but, on the contrary, a positive slope of 8% (10% in the work of Slevin *et al.*[27]). This indicates that the CEM does not work in the saturation mode; indeed, the pulse-height distribution shows that the peak is not completely separated from the background even for the highest voltage applied (4400 V) so that counts are lost by the electronics. The amount of the particle loss cannot be determined since a plateau is not observed and what can only be said is that there is a systematic underestimate of the cross section when use is made of such a CEM. In this work, systematic errors are eliminated by working always with the same potential applied to the CEM and by normalizing our cross sections to a reference value.

B. Errors and uncertainties

The reproducibility of the SDCS (after an integration over a line is made) given in this paper is generally within about ±15% when we consider the $({}^1S + {}^3P)$ and $({}^1D + {}^1P)$ lines. Additional uncertainties observed when we extract the separated contributions of the four lines by a numerical method are more difficult to evaluate; they strongly depend on the difficulties inherent to the numerical treatment which are discussed in the following section.

In order to determine the absolute error in our cross sections, we have to consider the uncertainties in the values of the parameters which enter the cross-section formula. Only the greatest errors will be considered; they come from the evaluation of the analyzer transmission t_a, detector efficiency η, and target density. The first two are obtained by a normalization as explained in the preceding section. The uncertainty in the combined parameter (ηt_a) includes that in the reference cross section (20% as given by Rudd *et al.*[24]), the target density (≤10%), the ion charge density (1%); the statistical error being neglected. When all these errors are combined in the rms fashion an error of 22% is obtained for the parameter (ηt_a). Then the uncertainty in the absolute values of our SDCS amounts to about 25%.

It must be noted that, above 50 keV, the numerical treatment of the energy spectrum gives the Shore parameter b (see Sec. III A) for which the above estimated error applies, whereas throughout this paper it is the quantity

$$\frac{d\mathcal{S}}{d\Omega} = \tfrac{1}{2}\pi\,\Gamma(2S+1)b \tag{1}$$

(where Γ and S designate, respectively, the level width and the spin of the autoionizing state), which is discussed. $d\mathcal{S}/d\Omega$ gives the algebraic surface of the asymmetrical structure observed in the ejected electron spectrum in the emitter frame; it has the same dimension as a single differential cross section. Its meaning will be discussed in the next section. Then an additional error is introduced in $d\mathcal{S}/d\Omega$ values by multiplying b by a Γ value which is not accurately known. The following values have been adopted for this parameter[28]: 0.14 ± 0.01, 0.010 ± 0.002, 0.070 ± 0.003, and 0.038 ± 0.002 eV, respectively, for the $2s^2\,{}^1S$, $2s2p\,{}^3P$, $2p^2\,{}^1D$, and $2s2p\,{}^1P$ resonances. The uncertainties in the Γ values result from the estimated dispersion of the published experimental and theoretical values. They do not markedly influence the error values given for b which may be applied to the $d\mathcal{S}/d\Omega$ for the singlet states; for $d\mathcal{S}({}^3P)/d\Omega$ the error rises up to about 32%.

All these considerations hold for the slow- as well as for the fast-particle SDCS. For the latter, another source of error may arise from the kinematic corrections (see Sec. IV B) it is necessary to apply to obtain SDCS values in the emitter frame; however as they are almost independent of the value of the unknown small scattering angle, they do not influence the error bars given above.

III. THE LINE SHAPE AND THE NUMERICAL ANALYSIS

The SDCS for each resonance $2s^2\,{}^1S$, $2s2p\,{}^3P$, $2p^2\,{}^1D$, and $2s2p\,{}^1P$ can only be obtained by a numerical treatment of the electron energy spectra on account of a too low analyzer energy resolution (0.67%) which does not allow a complete separation of the lines ${}^1D$ and ${}^1P$, ${}^1S$ and ${}^3P$. Even with a better resolving power a numerical analysis would be necessary because of the asymmetrical shape often observed which prevents any accurate determination of the line area by the more conventional planimetry method. A numerical analysis of the electron spectra requires an accurate knowledge of the various functions which contribute to the observed line profile. We shall first consider the

possible emission line shapes which might be observed in the emitter frame, and then the various kinematic effects which alter these emission line shapes when observed in the laboratory system. In Sec. III C will be discussed the numerical method used to obtain the separated contributions of the autoionizing lines considered in this paper.

A. Emission line shape

The electron line shape is mainly determined in our energy range (3–140 keV) by Fano interferences between the direct transition amplitude to the continuum and the autoionizing one as already observed in H^+ on He collisions[3,4] and explained by Balashov *et al.*,[2] and by PCI effects.[16]

1. PCI effect

In order to take into account the Coulomb interaction between the ejected electron and the nonemitting ion, we have two possibilities.

(a) First, the more general description of this effect at the present time was given by Morgenstern *et al.*[16] It allows for interference between transition amplitudes from the neighboring autoionizing levels $2s^2\,{}^1S$, $2p^2\,{}^1D$, $2s2p\,{}^1P$. However the theoretical energy distribution obtained in this way depends on a great number of parameters (excitation amplitudes, phases) and it becomes very difficult, when it is used for a numerical treatment of experimentally unresolved lines, to obtain reliable values for these parameters. Moreover as these interferences are only seen below 10 keV in He^+ on He collisions (an example at 7 keV is given in Gleizes *et al.*[17]; see also Ref. 16 where several examples are shown at collision energies lower than 5 keV), we have disregarded the possibility of this type of interference in our numerical treatment above 10 keV. Below this energy, no numerical analysis has been done and the unresolved line intensities have been obtained by planimetry.

(b) When the autoionizing levels are not coherently populated, the Barker and Berry classical distribution[18] is obtained as a particular case of the above general formulation. It was already used by us[19] to describe the line shape at 15 keV in He^+ on He collisions:

$$\frac{d^2\sigma_B}{d\Omega dE_0}=\frac{b_B\Gamma}{v(\Delta E)^2}\exp\left(\frac{\Gamma}{v\Delta E}\right), \tag{2}$$

the left-hand side is measured in a.u., where $\Delta E = E_0 - E_{0\infty}$, E_0 is the emission electron energy at finite R, $E_{0\infty}$ is the emission electron energy at infinite R, Γ is the atomic autoionizing state width (throughout this paper, it will be assumed to be independent of R), v is the collision velocity and b_B is the autoionizing state excitation probability which contains the angular dependence of the cross section:

$$\frac{d\sigma_B}{d\Omega}=\int dE_0\left(\frac{d^2\sigma_B}{d\Omega dE_0}\right)=b_B\,. \tag{2'}$$

The maximum of distribution (2) is shifted with respect to the resonance position $E_r \xrightarrow[R\to\infty]{} E_{0\infty}$:

$$E_M=E_r-\frac{\Gamma}{2v} \tag{3}$$

and its FWHM is given by

$$\Gamma_B=1.07\frac{\Gamma}{v}\,. \tag{3'}$$

Both E_M and Γ_B are measured in a.u.

Function (2) does not give the correct line profile at high collision velocity since, in the limit of large v, it tends to a delta function instead of a Lorentzian line $\mathcal{L}(E_0-E_{0\infty})$ with a finite FWHM Γ. In our first paper[19] this problem was solved by folding (2) by a Lorentz function. This method gives the correct line shape $\mathcal{L}(E_0-E_{0\infty})$ at large v but too broad a function $(\mathcal{L}*d^2\sigma_B/d\Omega dE_0)$ at low velocity [where (2) alone gives the correct energy distribution]. Physically we have made a classical addition of the intensities of every part of the line which contributes at E_0. In a quantal treatment of the autoionization at large R the amplitudes must be added; in this case Ostrovskii[29] and Devdariani *et al.*[30] have obtained a universal function which describes the line shape whatever the collision velocity is [an error of sign in the argument of the exponential term in formula (4.8) of Ref. 30 has been corrected in formula (4) of this paper.]:

$$\frac{d^2\sigma_D}{d\Omega dE_0}=\frac{b_D\Gamma}{\frac{1}{4}\Gamma^2+(\Delta E)^2}\,\frac{1}{2v\sinh(\pi/v)}\times\exp\left(\frac{\pi}{v}+\frac{2}{v}\arctan\frac{\Gamma}{2\Delta E}\right), \tag{4}$$

where the parameters have the same meaning as in (2). The excitation SDCS is given by

$$\frac{d\sigma_D}{d\Omega}=\int dE_0\frac{d^2\sigma_D}{d\Omega dE_0}=b_D\,, \tag{4'}$$

which will be simply noted $d\sigma/d\Omega$ in the following. Formula (4) gives the correct Lorentzian limit $\mathcal{L}$ when $v\to\infty$ and becomes similar to Barker and Berry's formula at low v. We have used (4) up to 50 keV. An example of agreement obtained at 10 keV is given in Fig. 2. Small discrepancies mainly remain on the low energy side of the $({}^1D+{}^1P)$ line which may be ascribed to PCI interference structures neglected in our treatment.

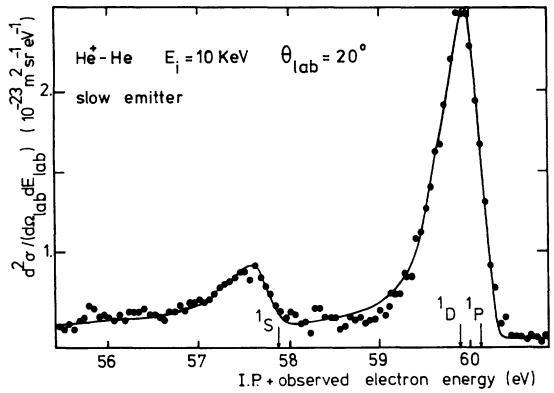

FIG. 2. Spectra of electrons ejected by autoionization of the slow particle in He^+ on He collisions at 10 keV and $\theta_{lab} = 20°$. The energy scale is calibrated against the $2p^2\,{}^1D$ energy state: 59.90 eV as obtained in Ref. 22. Energy resolution: 0.67% of the transmitted electron energy; channel width =0.055 eV. The continuous line is obtained by a fit of the experimental points (•) (see text).

2. *Fano's interferences*

The energy distribution (4) cannot be used to fit the experimental spectra above 50 keV because the lines have an asymmetry of the Fano type. As explained in Ref. 8, this line asymmetry is well described by Shore's function, which is more suitable to use in a fitting procedure than the well-known Fano formula

$$\frac{d^2\sigma_S}{d\Omega dE} = (2S+1)\frac{a\epsilon + b}{1+\epsilon^2}, \tag{5}$$

where S is the spin quantum number of the resonance,[31] $\epsilon = 2(E - E_r)/\Gamma$ is the reduced energy, E_r, and Γ being, respectively, the energy and width of the resonance. The resonance is described by the couple (a, b) of Shore's parameters: a defines the line asymmetry and b is proportional to the line area given by (1). The parameter b also contains, as b_B and b_D, the angular dependence of the cross section but it is important to remember that, in this case, b is not only a function of the electron angular momentum, as in (2) and (4), but also of interference terms between resonant and nonresonant transition amplitudes to the continuum. b may take positive, zero, or negative values, depending on the interference effect. Therefore it must be emphasized that although the quantity $d\mathcal{S}/d\Omega$, in (1), has the dimension of a single differential cross section, it generally differs from a true single differential *excitation* cross section $d\sigma/d\Omega$ of the autoionizing state. $d\mathcal{S}/d\Omega$ can only recover the meaning of an excitation cross section when the direct ionizing transition amplitude becomes small with respect to the autoionizing one; in this particular case $d\mathcal{S}/d\Omega \approx d\sigma/d\Omega$. An example of agreement between (5) and the experimental results is shown in Fig. 3.

It is interesting to compare the profile parameters $\tilde{q}$ of the ^1S resonance, at $\theta_{lab} = 20°$ when the helium atom is excited by a He^+ ion (140 keV, collision velocity $v \approx 1.18$ a.u.) or by a proton of equal velocity[8,25] (at 33 keV, $v \approx 1.15$ a.u.): $\tilde{q}$ (He^+) $= 2.4 \pm 0.5$, $\tilde{q}$ (H^+) ≈ -8. These results show that even for the highest energy studied in this paper, the helium ion is not equivalent to a unit charge structureless particle.

3. *PCI effect with direct transition to the continuum*

We cannot *a priori* disregard the possibility to have simultaneously a PCI effect and a direct transition to the continuum. Then the observed line shape will not be described either by (4) or by (5). Depending on the degree of coherence between the transition amplitudes to the different autoionizing states and between each autoionizing transition and the continuum,[32] various formulas may be used. Perhaps because of too large kinematic broadenings or rather because the direct transition amplitude to the continuum in He^+ on He collisions is only important above 50 keV where the PCI effect becomes negligible, we have never observed such an intermediate line shape.

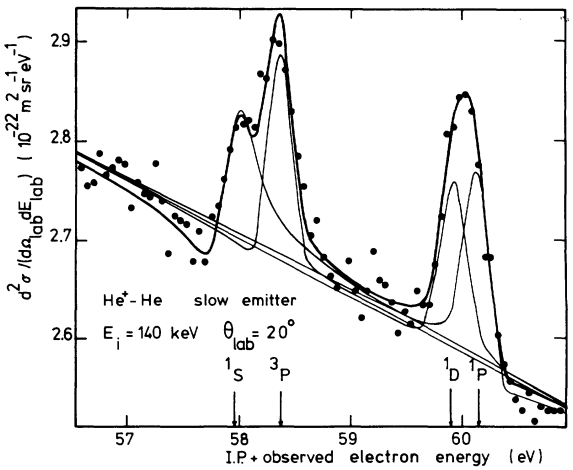

FIG. 3. Spectra of electrons ejected by autoionization of the slow particle in He^+ on He collisions at 140 keV, $\theta_{lab} = 20°$. The thin lines give the separated contributions of each autoionizing state. The other characteristics are the same as in Fig. 2, $\tilde{q}(^1S) = 2.4$, $\tilde{q}(^3P) = 15$, $\tilde{q}(^1D) = 22$, $\tilde{q}(^1P) = -7$.

Then the separation into two energy ranges, below and above 50 keV, for the ease of numerical analysis, seems to be well justified. Below 50 keV the line shape is described by (4) whereas above 50 keV (5) was preferred.

B. Kinematic broadenings

Many authors have discussed various kinematic broadenings. Some of them have already been quoted in a previous paper[19]; these effects are also discussed in Refs. 33–35. In this paper, we intend to discuss and make a quantitative evaluation of these broadenings in the particular case of the He^+-He collision, in our energy range.

When a study of the angular dependence of the SDCS is made, *the Doppler function* $\Phi_D(\phi)$, where ϕ is the azimuthal angle, gives the dominant kinematic broadening in the intermediate angular range, at low energy. This function has been determined in a rigourous manner by Gleizes *et al.*[19] for one value of the scattering angle θ_i of the emitter, assuming an isotropic azimuthal distribution about the incident beam direction of the ejected electrons with observed energy E_{lab}:

$$\Phi_D(\phi) \approx \frac{dN}{d\phi}\frac{d\phi}{dE_{\text{lab}}}, \tag{6}$$

with

$$\frac{dN}{d\phi} = \text{const} \tag{6'}$$

and $d\phi/dE_{\text{lab}}$ is given by relation (17) in Ref. 19.

The assumption (6′) is always verified in noncoincident experiments when use is made of unpolarized incident beam and target[13,33,36,37]; it does not depend on the angular momentum of the autoionizing state considered. In coincident experiments, on the other hand, a direction normal to the incident beam is defined and the angular distribution depends[36,37] on ϕ; this has been observed, for example, by Kessel *et al.*[38] In the case of autoionization of the helium atom, the distribution $dN/d\phi$ depends on the angular momentum of the autoionizing state (since the ion after autoionization is left in an S state, the angular momenta of the ejected electron and excited state are identical) since it is given by

$$\frac{dN}{d\phi} = \left| \sum_{M_L} a_{M_L} Y_{L M_L}(\theta, \phi) \right|^2 \tag{6''}$$

for a given emission angle θ. In (6″) a_{M_L} stands for the excitation amplitude of the excited level (L, M_L), where M_L is the projection of the angular momentum on to the incident beam axis. The right-hand expression is given, for example, by Eqs. (11) and (12) in Ref. 38 for the ^1D and ^1P autoionizing states, respectively. Relation (6′) is also consistent with the fact that in noncoincident experiments, the excited state must be represented by an incoherent superposition of pure states with different quantum numbers[37] M_L; on the contrary, the azimuthal anisotropy in coincident experiments comes from the coherent superposition in (6″) which gives rise to interference terms (with odd powers of $\cos\phi$) between various magnetic sublevel amplitudes.[39]

In our noncoincident experiment, *all the emitter scattering angles* θ_i *contribute* and this induces a broadening $\Gamma_D(\theta_i) = (\partial E_{\text{lab}}/\partial\theta_i)\Delta\theta_i$ of the electron lines. The authors who first mentioned this effect have already been mentioned in our previous paper[19]; Stolterfoht *et al.*[34] also discussed this broadening but in Eq. (33) of their paper E_{e0}, instead of E_{lab}, is incorrectly derived with respect to θ_i. To take into account in our numerical treatment such a broadening, it would be necessary to roughly know the θ_i angular distribution which contributes to the excitation of the autoionizing states considered in this paper. The only published experimental results which give this distribution in our energy range are those of Bordenave-Montesquieu and Dagnac[40,41] who show that scattering angles higher than $\theta_i = 3°$ do not give a significant contribution to the 60-eV energy loss peak at 10 keV. Thus the maximum broadening is evaluated by taking $\Delta\theta_i = 3°$ and by considering that the most probable angle (noted θ_i^*) is equal to $\theta_i^* \approx 1°$; thus we get $\Gamma_D(\theta_i^*) \lesssim 20$ meV. For higher incident particle energies, $\Gamma_D(\theta_i)$ is even smaller because θ_i^* and $\Delta\theta_i$ decrease.[40]

The analyzer acceptance angle gives an additional broadening which is only observable in the electron spectra emitted by the fast particle. It is maximum for angles θ_{lab} smaller than 90° and becomes considerable at high impact velocities. This effect has been described in detail in a previous paper.[42] For a given θ_{lab}, its maximum value is given by

$$\Gamma_D^M(\theta_{\text{lab}}) = \left(\frac{\partial E_{\text{lab}}}{\partial \theta_{\text{lab}}}\right)\Delta\theta_{\text{lab}}.$$

The derivative may be found in Ref. 33; it may also be obtained from Eq. (9) in Ref. 19. Stolterfoht *et al.*[34] have also discussed this broadening but an incorrect derivation of E_{e0}, instead of E_{lab}, against θ_{lab} has been made in this paper. This broadening is always large ($\Delta\theta_{\text{lab}} = 2.4°$ in our experiment) except in the forward and backward directions. It roughly varies with θ_{lab} as $\Gamma_D(\phi)$ (defined in Ref. 19) does; however the collision energy dependence is very different since $\Gamma_D(\phi)$ turns out to be negligible for the highest energies studied in this paper whereas $\Gamma_D(\theta_{\text{lab}})$ increases very fast: at

140 keV, near 50° the structures ($^1S + {}^3P$) and ($^1D + {}^1P$) begin to merge together (the distance ^1S-^1D is equal to 2.04 eV). In these conditions the original contribution of each line becomes quite difficult to recover and the accuracy of the fast atom cross sections at 100 and 140 keV is certainly very bad. An example of fit obtained when the acceptance function defined in Ref. 42 is used, is given at 100 keV ($\theta_{lab} = 30°$) in Fig. 4 (another example obtained in He^0+He collisions is given in Ref. 42). The numerical method used to attempt to obtain significant SDCS for the ^1S, ^3P, ^1D, and ^1P lines, even in the fast atom spectra at high energy, will be examined now.

C. Numerical method

The accuracy of the excitation cross-section values not only depends on the measurement of various experimental parameters as explained in Sec. II B but also of the case taken to do the numerical treatment of the electron spectra. Only the most important points of the method will be discussed here; more details can be found elsewhere.[43]

1. The adjustment of the theoretical line shape $y_t(E_{lab}, p_j)$ and the experimental spectra $y_{expt}(E_{lab})$. The adjustment of the theoretical line shape $y_t(E_{lab}, p_j)$ and the experimental spectra $y_{expt}(E_{lab})$ is made by means of a least-squares-fit method which permits us to adjust the parameters p_j. If the theoretical line shape depends linearly on the various parameters p_j, the quantity $(y_t - y_{expt})^2$ is quadratic on p_j and in this favorable case the program approaches immediately the exact solution p_{j0} for this parameter, whatever the input value p_{j1} is. On the contrary when the dependence of y_t on p_j is not linear, it will be necessary to choose p_{j1} close to p_{j0} in order that the parabolic interpolation gives the true solution p_{j0}. Of course, in this case large errors may happen if the input value is not correctly chosen and the uniqueness of the solution is never achieved. In our case y_t depends linearly on the intensity b, the Shore parameter a and the parameters of the straight line which approximate the continuous background in the electron spectra; on the contrary, a more complex dependence is obtained for the resonance energies. For the former parameters we always take arbitrary input values whereas it is necessary to determine as accurately as possible the input values of the resonance position; practically, several input values are tried for the resonance positions.

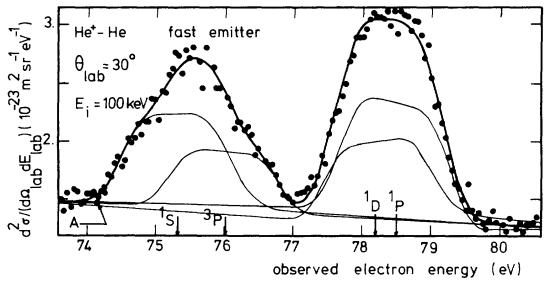

FIG. 4. Influence of the broadening $\Gamma_D(\theta_{1ab})$ on the lines issued from the fast particle at 100 keV, $\theta_{lab} = 30°$ ($\theta^*_{em} = 48.3°$). Point A serves to find the ^1S line position as explained in the text. The heavy line gives the best fit obtained with the experimental points (•); the thin lines give the separated contributions of each autoionizing level. The analyzer energy resolution is equal to 1.1% of the transmitted electron energy; the channel width is equal to 0.058 eV. The abscissa is calibrated against the ^1D position; the ^1D-^1P distance is kept constant and equal to 0.360 eV [this value includes the Doppler shift and takes into account the different Doppler shift values for 35.32 eV (^1D) and 35.55 eV (^1P) electrons].

2. The theoretical function y_t. The theoretical function y_t must be accurately known in order that the least-squares fit gives a meaningful solution. The uniqueness of the solution is strongly related to the quality of the fit and, hence, to the knowledge of y_t. y_t results from successive convolutions of PCI function (4) or Shore's function (5), depending on the collision energy considered, by the Doppler function $\Phi_D(\phi)$ defined in Ref. 19 [Eq. (17)] and by the trapezoidal analyzer function; the width of the latter is proportional to the slit width used (Sec. II A) and to the observed electron energy E_{lab}. When fast-particle electron spectra are studied, a convolution by the acceptance function defined in Ref. 42 must also be made. All the above functions have been defined as accurately as possible; however, their practical use if often not easy. Various difficulties have been encountered with $\Phi_D(\phi)$.

It depends on the emitter scattering angle θ_i^* (defined in Sec. II B) which is unknown in a noncoincident experiment (Sec. III B). Various tests have been made at 10 keV and finally the value $E_i\theta_i^* = 8$ keV deg, where E_i the collision energy has been chosen whatever the collision energy is; this value is in good agreement with the results obtained in inelastic scattering experiments for the He^+-He collisional system at 10 keV.[40] Since θ_i^* decreases when the collision energy increases[40,41] and the Doppler broadening $\Gamma_D(\phi)$ varies in the same way, it is only important to make the good choice for θ_i^* at the lowest energy (10 keV).

The rigorous convolution by $\Phi_D(\phi)$ must be made along the following method at each point E_{e0} of the

emission electron spectra: Calculate $\Phi_D(\phi)$ for this E_{e0} value and translate it to an observed electron energy value E_{lab}. Then, as $\Phi_D(\phi)$ and the Doppler shift Δ_D depends on E_{e0}, this method becomes computer time consuming if we consider that an electron energy range of about 5 eV is analyzed with a theoretical energy step of about 0.01 eV. We have verified that the following approximate method still gives a correct result.

$\Phi_D(\phi)$ is only calculated once for the mean electron energy value $\overline{E}_{e0}=34.4$ eV in the slow electron spectra, and for $\overline{E}_{e0}+\Delta_D(\overline{E}_{e0})$ for the fast electron spectra, neglecting its variation against E_{e0}.

For the fast electron spectra, the variation of Δ_D with E_{e0} [Eq. (9) in Ref. 19] is assumed to be negligible along a line width. However, the variation of Δ_D along the 5-eV width of the electron spectra is *not* negligible and this will be taken into account in the determination of the distance between the resonances.

3. *The distance between the resonances.* The distance between the resonances must be known accurately. This parameter has a crucial importance when two lines, like $2p^2\,{}^1D$ and $2s2p\,{}^1P$, are not resolved in the experimental spectra. The following values have been adopted for the slow electron spectra[22] $E_r({}^3P)=E_r({}^1S)+0.50$ eV, $E_r({}^1D)=E_r({}^1S)+2.05$ eV, $E_r({}^1P)=E_r({}^1D)+0.23$ eV where E_r is the resonance value. A comparison of our values (except that of the $2s2p\,{}^3P$ one), with all the other experimental or theoretical ones made by Shearer-Izumi[44] shows that our own values are in very good agreement with the more accurate experimental ones. The ${}^3P$ and ${}^1D$ lines are linked to the ${}^1S$ position whereas the ${}^1P$ line is linked to the ${}^1D$. If all these distances are kept constant, it has often been observed that the best fit is not obtained. Then, in a practical case, a fit is first obtained with these input values and, after that, the ${}^1S$-${}^1D$ distance is allowed to vary within generally one channel width (±0.06 eV); the ${}^1S$-${}^3P$ distance is only allowed to vary within the same limits when the ${}^3P$ line is not too small with respect to the ${}^1S$. On the other hand, the ${}^1D$-${}^1P$ distance must be kept constant in order to prevent erroneous results resulting from a position exchange between the ${}^1D$ and ${}^1P$ lines. For the fast electron spectra, we know that the Doppler shift Δ_D depends on E_{e0}; neglecting the variation of Δ_D along a line width, we have taken into account the variation of the line distances due to this E_{e0} dependence (in eV) as follows:

$$E_r({}^3P)=E_r({}^1S)+0.50+\Delta_D({}^1S-{}^3P)\,,$$

$$E_r({}^1D)=E_r({}^1S)+2.05+\Delta_D({}^1S-{}^1D)\,,$$

$$E_r({}^1P)=E_r({}^1D)+0.23+\Delta_D({}^1D-{}^1P)\,,$$

where $\Delta_D({}^1S-{}^3P)$, for example, means that we calculate the difference of the Doppler shifts $\Delta_D(E_r({}^1S))$ and $\Delta_D(E_r({}^1P))$.

4. *The ${}^1S$ resonance position.* The ${}^1S$ resonance position is the last parameter which has a great influence on the validity of the solution of the least-squares-fit procedure. From the experimental spectra we only have the maximum position of the ${}^1S$ line $E_M({}^1S)$. Below 50 keV the input resonance position $E_r({}^1S)$ is recovered by using relation (3) which also applies when (4) is used.[30] Above 50 keV, the Fano asymmetries are generally so small that we assume that $E_r({}^1S)\approx E_M({}^1S)$ for the imput value.

A more difficult problem happens for the fast-particle spectra above 50 keV related to the great broadening due to the acceptance function. In this case even the $E_M({}^1S)$ value is difficult to recover with a reasonable accuracy. However if we note that the low-energy wing of the ${}^1S$ line is never perturbed by the ${}^3P$ when no Fano asymmetries are present, the ${}^1S$ maximum is obtained by the following method: In each case, we determine the function resulting from folding in together the acceptance and apparatus functions, neglecting Shore's function, and we measure its base width ΔE_b; the ${}^1S$ line position is then taken at the distance $\Delta E_b/2$ from the beginning of the low-energy wing of the ${}^1S$ line (point A in Fig. 4). Under these conditions we believe we will obtain the ${}^1S$ position within 0.1 to 0.2 eV.

IV. ANGULAR DISTRIBUTION

A. Theoretical considerations

From the work of Cleff and Mehlhorn,[13] the angular dependence of the SDCS measured in this work has already been established elsewhere[14] in the case of electron emission by an isolated atom without allowance for any kind of angular perturbations. It must be noted that Cleff and Mehlhorn's formulation explicitly assumes that the fine-structure splitting is large compared to the level width, when the spin-orbit interaction is rather high, so that it applies to excitation of high Z atoms for which the $(LSJM)$ coupling scheme must be used. On the other hand, for light atoms, this is no longer true and the (LSM_LM_S) scheme must be applied (no spin-orbit interaction, fine-structure splitting much smaller than the level width); the theoretical expression which applies in this latter case has been established in our previous paper[14] using the method of Cleff and Mehlhorn.[13] The SDCS (4a) has the following form, in the emitter reference frame:

$$\frac{d\sigma}{d\hat{\Omega}}\approx\sum_{M_L}P(L,M_L)\,|\,Y_{L,M_L}\,|^2\,, \tag{7}$$

where $P(L, M_L)$ is the excitation probability of the sublevel (L, M_L) of the excited state and M_L is the projection of the angular momentum on the incident beam axis. Equation (7) can also be put in a more practical form:

$$\frac{d\sigma}{d\Omega} \approx \sum_{j=0}^{L} a_j \cos^{2j}\theta , \qquad (7')$$

where θ is the emission angle defined in the emitter frame; the a_j coefficients depend on the sublevel populations $P(L, M_L)$ of the excited state. Equation (7), or (7'), is only valid for noncoincident experiments where the excited state is represented by an incoherent superposition of pure state with different magnetic quantum numbers M_L.[37] This expression contrasts with the one used by Kessel *et al.*[38] in the case of coincident experiment; in this case, a coherent superposition must be taken. Squaring the transition amplitudes given by Eqs. (11) or (12) in Ref. 38, it appears interference terms between excitation amplitudes to different magnetic sublevels of the same excited state, generally makes the angular distribution in coincident experiments no more symmetrical with respect to $\theta = 90°$, contrary to (7) or (7').

It must be kept in mind that a PCI distortion of the line shape is observed up to 50 keV which indicates that the electron is not emitted by an isolated atom and that it suffers the influence of the Coulomb field of the nonemitting ion. A helium atom of 10 keV energy has traveled about 60 to 220 a.u. when autoionization occurs depending on the autoionization lifetime (10^{-14}–10^{-15} s), so that a molecular distorsion of the electron cloud[45] may certainly be considered as a weak effect above 10 keV. At lower collision velocities ^1S-^1D, ^1S-^1P, and ^1D-^1P PCI interferences destroy the angular dependence given by (7) as can be seen by integrating Eq. (1) in Ref. 38 over the azimuthal angle and the electron energy. The resulting angular distribution which takes into account these PCI interferences between the ^1D and ^1P sublevels would be more complicated than that given by Eq. (7') for $L = 2$; it also contains odd power cosines coming from crossed terms. Then, generally, asymmetrical angular distributions with respect to $\theta = 90°$ must result from this post-collision perturbation.

We must also note that the Coulomb field of the ion produces a Stark mixing of the same M_L substates of the ^1D and ^1P states which induce asymmetrical angular distributions.[20] As for the PCI effect, this Stark effect is only important at low collision velocity, certainly below 10 keV.

Finally when interferences between resonant and all the nonresonant transition amplitudes to the continuum become important, the measured quantity is $d\$/d\Omega$ [given by (1)] instead of the excitation cross section $d\sigma/d\Omega$, and it generally does not obey any longer the angular variation given by (7'). Owing to the odd power cosines coming from the various interference terms it will result in an angular dependence asymmetrical against $\theta = 90°$.

In practice, the analysis of the angular distributions has been separated in two cases.

(1) When symmetrical angular distributions are observed, relation (7') can be used. By a numerical fitting procedure between (7') and the experimental points corrected for kinematic effects as indicated in the next section, we obtain a_j parameters and hence the relative sublevel populations $P(L, M_L)$. For the D state, we used the following formulas: (In (8) some misprints contained in Ref. 14 [relations (3a) to (3c)] are corrected.):

$$\begin{aligned} P(2,0)/P_T &= 3(a_0+a_1+a_2)/(15a_0+5a_1+3a_2) , \\ P(2,1)/P_T &= (3a_0+2a_1+a_2)/(15a_0+5a_1+3a_2) , \\ P(2,2)/P_T &= (3a_0-a_1-a_2)/(15a_0+5a_1+3a_2) , \end{aligned} \qquad (8)$$

where $P_T = P(2,0) + 2P(2,1) + 2P(2,2)$ is the total population of the excited state. In a similar way the expressions for the P states are given by

$$\begin{aligned} P(1,0)/P_T &= (a_0+a_1)/(3a_0+a_1) , \\ P(1,1)/P_T &= a_0/(3a_0+a_1) , \\ P_T &= P(1,0) + 2P(1,1) . \end{aligned} \qquad (9)$$

The S states give of course isotropic electron distributions.

(2) For asymmetrical experimental curves, which show the influence of a perturbation as discussed above, an arbitrary polynomial containing odd powers has been used:

$$\frac{d\sigma}{d\Omega} = \sum_{j=0}^{4} a_j \cos^j\theta . \qquad (10)$$

A comparison with the experimental results show that no higher power than $j = 4$ is necessary. The fit of the experimental points with (10) allows us to obtain in an easy way the total cross section through analytic integration.

The experimental SDCS ($d\sigma/d\Omega$ or $d\$/d\Omega$) defined in the emitter frame are obtained from the same quantities measured in the laboratory frame through the kinematic transformation (13) which will be defined in the following section.

B. Kinematic corrections

From the values measured in the laboratory system (observation angle, cross section) the corresponding quantities in the emitter frame must be calculated. As explained by Gleizes *et al.*,[17] the frame attached to the emitter must be

defined in the center of mass (c.m.) system: The emission angle is then defined with respect to the internuclear axis direction as shown in Fig. 5 (it is supposed that only one θ_i value contributes). We will only give the results for the kinematic corrections. From Fig. 5(b), we see that the emission angle θ^s_{em} for the slow emitter is approximately given by

$$\theta^s_{em} \approx \pi - \theta_{lab}\,, \tag{11}$$

where θ_{lab} is the observation angle; this approximation holds for small values of the scattering angle θ_i of the projectile.

A more complicated expression is found for the fast emitter (within the elastic collision approximation):

$$\cos\theta^f_{em} = \frac{v_i}{v_{e0}}[\cos\theta' \cos 2\theta_i(\cos\theta' + \alpha) - \cos^2\theta_i]\,, \tag{12}$$

with

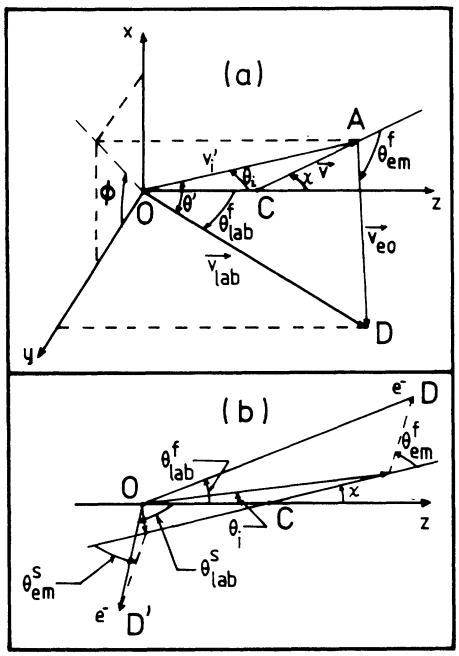

FIG. 5. Kinematics of the collision. (a) Fast emitter parameters. (b) Correspondence fast or slow emitter angles. All the velocity vectors and angles involved in the various kinematic effects are given; the subscript lab identifies the quantities observed in the laboratory frame and em in the emitter frame (except for the emission electron velocity which is noted v_{e0}). C is the center of mass. v'_i is the fast particle velocity after the collision in the laboratory frame.

$$\alpha = \left[\left(\frac{v_{e0}}{v_i \cos\theta_i}\right)^2 - \sin^2\theta'\right]^{1/2}.$$

$\cos\theta' = \cos\theta_i \cos\theta_{lab}$ when averaged over the azimuthal angle ϕ. v_i designates the velocity of the incident particle and v_{e0} the electron velocity in the emitter frame.

As θ^f_{em} is almost independent of the small value of θ_i, θ^f_{em} may be calculated with $\theta_i = 0°$. The values θ^f_{em} given by (12) are almost identical to those calculated with another definition of the emission angle[14,45]: The reference axis was taken in Refs. 14 and 45 as given by the projectile scattering direction instead of the internuclear axis. However, as θ_i is always small, the difference between the two kinds of results is always very small.

The measured cross section $d\sigma/d\Omega_{lab}$ is related to the SDCS in the emitter frame by the relation

$$\frac{d\sigma}{d\Omega_{em}} = \frac{d\sigma}{d\Omega_{lab}}\frac{d\Omega_{lab}}{d\Omega_{em}}\,. \tag{13}$$

Equation (13) will be designated by $d\sigma/d\Omega$ in the following. The same relation holds between $d\mathcal{S}/d\Omega_{em}$ (noted $d\mathcal{S}/d\Omega$) and $d\mathcal{S}/d\Omega_{lab}$. For the fast emitter, the solid angle correction $d\Omega_{lab}/d\Omega_{em}$ is given by

$$\left(\frac{d\Omega_{lab}}{d\Omega_{em}}\right)^f = \left[\frac{v_i}{v_{e0}}\cos\theta_i \cos 2\theta_i \alpha^{1/2}\left(1 + \frac{\cos\theta_i \cos\theta_{lab}}{\alpha^{1/2}}\right)^2\right]^{-1}. \tag{14}$$

We must mention that when it becomes higher than a few units, the measurement of the fast emitter cross section is very difficult; this mainly occurs at 100 and 140 keV for great observation angles. As for θ^f_{em}, the difference with the values previously used[14] is small. For the slow emitter cross section, the solid angle correction is always given by

$$\left(\frac{d\Omega_{lab}}{d\Omega_{em}}\right)^s \approx 1\,. \tag{15}$$

C. Results and discussion

The angular distributions obtained between 3 and 140 keV are given in Figs. 6–12. Above 10 keV the results concerning the $2s^2\,{}^1S$, $2s2p\,{}^3P$, $2p^2\,{}^1D$, and $2s2p\,{}^1P$ lines have been obtained by the numerical method described in Sec. III C; the $2p^2\,{}^1S$ cross section is measured by planimetry. Below 10 keV, only planimetry has been used so that the $({}^1D + {}^1P)$ contribution alone can be measured (Fig. 11); the $2p^2\,{}^1S$ and $2s^2\,{}^1S$ cross sections have been only obtained at 7 keV. The excitation of the $2s2p\,{}^3P$ line

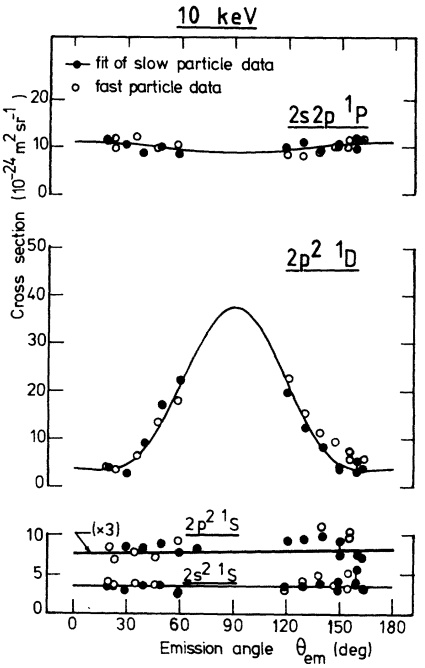

FIG. 6. Angular distributions of the electrons emitted by the $2s^2\,{}^1S$, $2p^2\,{}^1D$, $2s2p\,{}^1P$, and $2p^2\,{}^1S$ autoionizing states at 10 keV. Only the fit of the slow-particle data (•) with relation (7′) is given by a continuous line; the fast-particle data are represented by open circles (○) and show that equal SDCS are obtained for the two particles in the emitter frame.

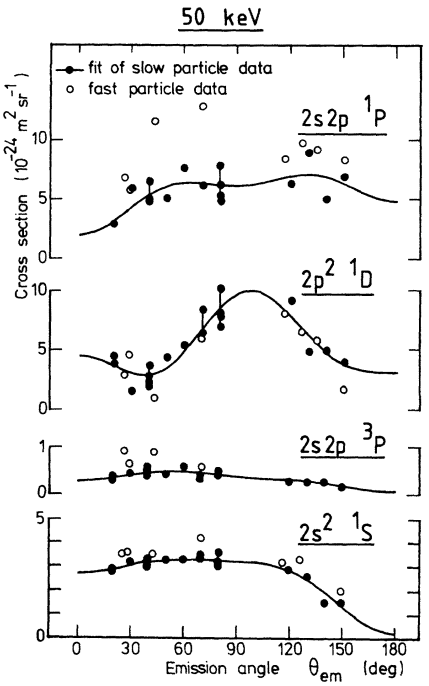

FIG. 8. Same as Fig. 7 at 50 keV. The discrepancies between the fast- and slow-particle SDCS for the ^1P line must be noted.

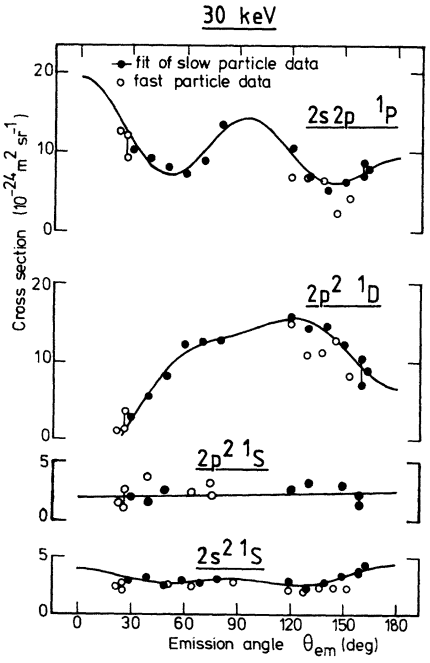

FIG. 7. Same as Fig. 6 at 30 keV. The fit of the slow-particle data is obtained with relation (10).

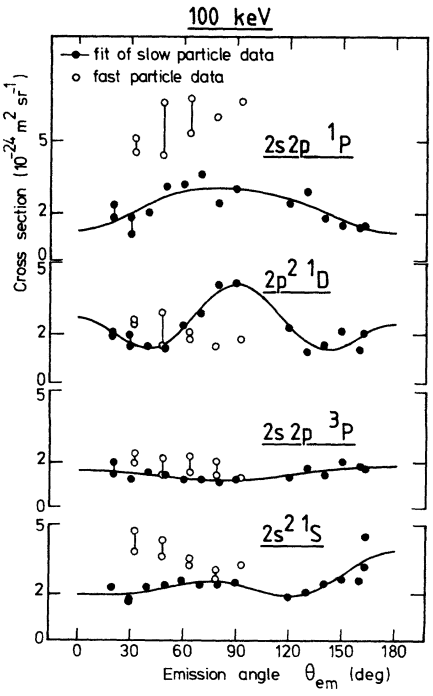

FIG. 9. Same as Fig. 7 at 100 keV.

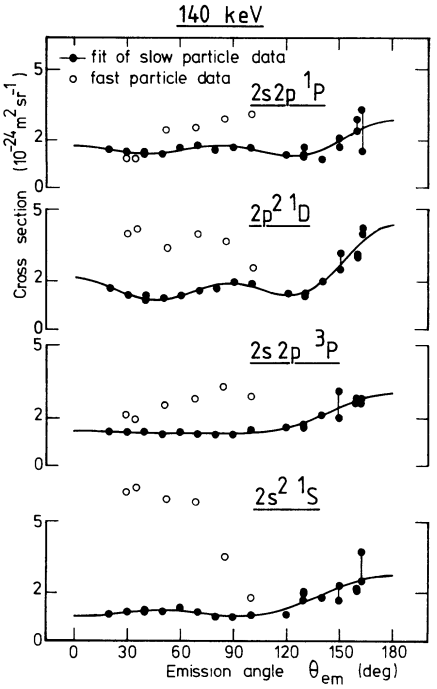

FIG. 10. Same as Fig. 7 at 140 keV.

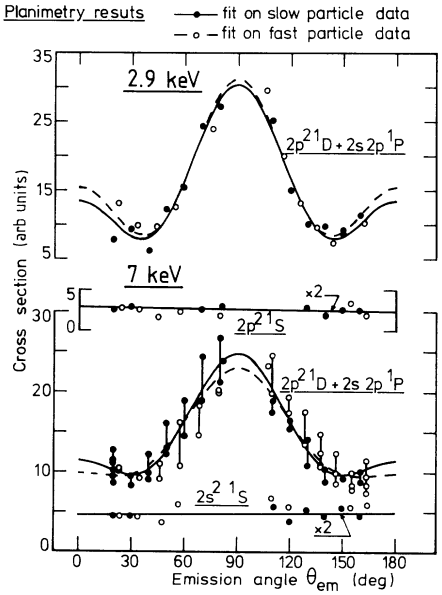

FIG. 11. Angular dependence of the $(2p^{2}\,{}^{1}D + 2s2p\,{}^{1}P)$ line as measured by planimetry at 2.9 and 7 keV. The $2s^{2}\,{}^{1}S$ values are certainly affected by PCI interference with the ^{1}D and ^{1}P states (see the energy spectra given in Ref. 17 at 7 keV). The fit is obtained with relation (7′).

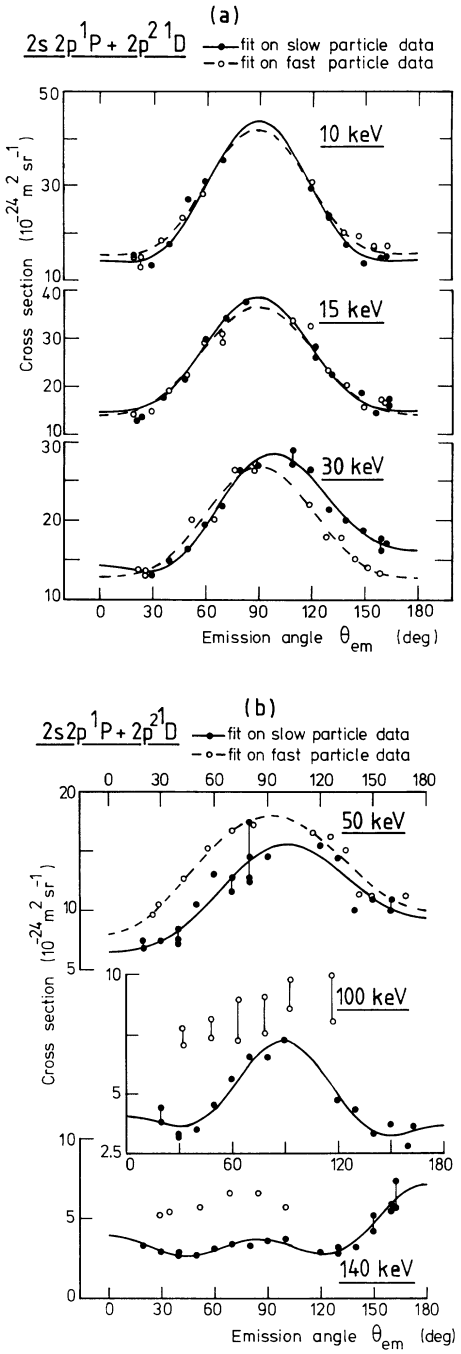

FIG. 12. Angular dependence of the $(2p^{2}\,{}^{1}D + 2s2p\,{}^{1}P)$ line. The separated fits of the fast-particle data (broken lines) and slow-particle data (continuous line) are obtained with relation (7′) at 10 and 15 keV and with relation (10) at 30 keV and above. (a) Results obtained at 10, 15, and 30 keV. (b) 50, 100, and 140 keV data. The asymmetry of the angular distributions with respect to $\theta_{em} = 90°$ and the difference between fast- and slow-particle SDCS values are clearly seen at 30 keV and above.

has not been observed below 30 keV; even at 30 keV this excitation is too weak to give reliable results. The full curves in these figures result from a least-squares fit of the experimental values with the analytical form (7′) below 15 keV and with formula (10) at 30 keV and above. No experimental results can be obtained around $\theta_{em} = 90°$, especially below 50 keV, because fast- and slow-particle electron spectra are superimposed on each other.

1. Angular distributions

The angular distributions can give information on *the population of the magnetic sublevels* of the autoionizing states whenever they are symmetrical with respect to $\theta_{em} = 90°$ and they have the correct angular dependence.[14] In Fig. 6 this is well verified for all the lines at 10 keV (the same holds at 15 keV). We note that the excitation of the ^1P line is preponderant for small and large θ_{em} values whereas the ^1D line excitation predominates around $\theta_{em} = 90°$; at this energy, the isotropic variations of the $2p^2\,^1S$ and $2s^2\,^1S$ distributions are also well verified. Below 10 keV (Fig. 11), the fit of the $(^1D + ^1P)$ distribution has been made with the assumption that the ^1P line is weakly excited. In order to test the validity of this assumption, the ratio of the ^1D and ^1P cross sections obtained at 10 keV in the present work can be compared with those measured by Morgenstern *et al.*[16] and Kessel *et al.*[38] First we can compare the SDCS values obtained at $\theta = 180°$ where only the $^1D(M_L = 0)$ and $^1P(M_L = 0)$ sublevels contribute: $[d\sigma(^1P)/d\Omega]/[d\sigma(^1D)/d\Omega] = 3.1$ in the present work at 10 keV (Fig. 6), 0.25 in Ref. 16 at 1.4 keV (noncoincident experiment), 0.09 in Ref. 38 at 2 keV, $\theta_i = 6°$ (coincident experiment). We can also compare the total cross sections anticipating on the values obtained in this work (Sec. V and Table II), $\sigma_{tot}(^1P)/\sigma_{tot}(^1D) = 0.48$ in the present work at 10 keV, 0.03 in Ref. 38 at 2 keV, $\theta_i = 6°$. All these comparisons show a much stronger ^1P excitation at 10 keV than at 2 or 1.4 keV. Therefore, the neglect of the ^1P excitation in the analysis of our angular distributions below 10 keV seems a better assumption at 2.9 keV than at 7 keV. Let us now consider all the relative sublevel populations obtained below 15 keV which are given in Table I; we can compare them with the results of Kessel *et al.*[38] obtained at 2 keV by a coincidence experiment and with our first results[14] obtained at 15 keV by planimetry assuming that the ^1P state is not excited. All these results are in rather good agreement. As we obtain the same values for two different sets of spectra, the slow and fast emitter ones, we may think that our results are rather accurate. They show that for the ^1D state the $|M_L| = 2$ sublevel is almost exclusively excited with a percentage varying between 70 to 90%; the $|M_L| = 1$ and $M_L = 0$ excitations are almost the same in our results. For the ^1P state, at 10 and 15 keV, the $|M_L| = 1$ sublevel is also the most excited but the difference between the two sublevel excitations is not as significant as that observed for the ^1D state be-

TABLE I. Relative sublevel populations for the $2p^2\,^1D$ and $2s2p\,^1P$ states of helium measured in He^+ on He collisions. The labels F and S mean that the fast- or slow-particle excitations are considered only.

Collision energy (keV)			2[a]	2.9[b]	7[b]	10[d]	15[b,c] (Ref. 3)	15[d]
$2p^2\,^1D$	$\frac{2P(2,2)}{P_T}$	S	0.63	0.80	0.70	0.94	0.65	0.90
		F		0.78	0.68	0.85		0.87
	$\frac{2P(2,1)}{P_T}$	S	0.26	0.05	0.16	0.03	0.23	0.03
		F		0.05	0.20	0.11		0.08
	$\frac{P(2,0)}{P_T}$	S	0.11	0.15	0.14	0.03	0.12	0.07
		F		0.17	0.12	0.04		0.05
$2s2p\,^1P$	$\frac{2P(1,1)}{P_T}$	S	0.80			0.61		0.66
		F				0.58		0.64
	$\frac{P(1,0)}{P_T}$	S	0.20			0.39		0.34
		F				0.42		0.36

[a] Coincidence experiment of Kessel *et al.* (Ref. 38).
[b] These results assume that the ^1P state is not excited (angular distributions obtained by planimetry).
[c] The whole results (S+F) have been fitted in Ref. 14.
[d] The results given in Ref. 15 are in error.

cause we seen in Fig. 6 that, within an error bar of about ±20% the ^1P angular distribution may be also considered as isotropic (equality of the $|M_L| = 1$ and 0 populations). For this state our results above 10 keV differ from those obtained by Kessel *et al.* which give a meaningful preponderance of the $|M_L| = 1$ excitation. These authors compare their results at 2 keV with our own values[14] obtained at 15 keV neglecting the ^1P excitation; the agreement is surprisingly good and fortuitous since we actually know that our previous assumption that the ^1P state is not excited, is wrong. The excitation mechanisms will be discussed in Sec. V. Let us consider now *the evolution of the angular distributions with collision energy*. Below 15 keV all the angular variations are symmetrical with respect to $\theta_{em} = 90°$ [Figs. 6, 11, and 12(a)]. This result is not obvious since, at least at 2.9 and 7 keV, PCI interferences between the autoionizing amplitudes of the $2s^2\,^1S$, $2p^2\,^1D$, and $2s2p\,^1P$ states perturb the observed line shape (see Fig. 1 in Ref. 17 where spectra obtained at 7 keV are given). As explained above in Sec. IV A, they can destroy the symmetry of the angular distribution. Such a perturbation is not observed in Fig. 11 since a good fit of the experimental results is obtained with (7′); for this reason we may think that the PCI interference does not seriously affect the population values given in Table I. The Stark effect,[20] which can perturb too the angular distributions at low collision energy, seems to also have no effect on the observed distributions. Above 30 keV the angular distributions are no longer symmetrical [Figs. 7–10, 12(a), and 12(b)].

If the PCI interference and Stark effect do not perturb the curves at low collision energy, they cannot explain *a fortiori* the asymmetrical curves observed above 30 keV since the influence of the Coulomb field of the He^+ ion on the autoionization of the He atom decreases as the relative collision velocity increases. In our opinion, the results are qualitatively similar to those obtained in $H^+ + He$ collisions[8] and can be explained in the same way. This asymmetry is due to the occurrence of a direct transition to the continuum which competes with the autoionizing one. In these conditions, Balashov *et al.*[2] have shown that interference terms between the resonant and all the nonresonant partial waves of the continuum appear in the term b [Eqs. (1) and (5)] which describes the line intensity; then the angular dependence of $d\$/d\Omega$ is not given by (7′). Moreover, we must recall that Fano line shapes are not always observed simultaneously with a perturbed angular distribution[8,45] since the parameters a [Eq. (5)], which describes the line asymmetry, and b behave in a different way as they contain different interference terms: It is then possible that, at 30 and 50 keV, the angular distributions should be affected whereas the lines do not have the typical Fano form. This means that even if the line shapes obey the PCI form given by (4), the line intensities may be perturbed by these interferences. Therefore, in this case, the line area no longer gives the true cross section $d\sigma/d\Omega$ but instead the quantity $d\$/d\Omega$ which is effectively obtained even if Shore's parametrization is not necessary to describe the line shape. Above 100 keV this interpretation is supported by the simultaneous observation of asymmetrical Fano line shapes (Fig. 3) and perturbed angular distributions [Figs. 9, 10, and 12(b)]. The origin of the direct excitation of the continuum cannot be made completely clear with our results alone. The continuum may be populated in two different ways. The first one might be due to a molecular autoionization of the entrance channel $A\Sigma_g$ at short internuclear distance[46] ($R \leq 1.2$ a.u.).[47] Since this state is correlated at $R = 0$ to the $Be^+(1s2p^2)$ autoionizing united atom configuration, more than 100 eV above the ionization limit $Be^{2+}(1s^2)$ to which is correlated the molecular ionization limit $(1s\sigma_g)^2\,^1\Sigma_g$, electrons of about 33–35 eV may well be emitted by autoionization. The condition of coherence of the continuum and atomic autoionizing state excitation would be verified with this mechanism since the two competing channels will be excited by the same $A\Sigma_g$ source in the same collisional event. ($\lambda = 0$) electrons are produced by autoionization of the $A\Sigma_g$ state if the electrostatic coupling is only considered or ($\lambda = 0, 1$) electrons when dynamic couplings (radial, rotational) are involved.[47] Following the interpretation given by Kessel *et al.*,[38] the rotational coupling could provide a $\lambda = 0, 1, 2$ excitation. The discussion of this interpretation will be delayed until Sec. VI. The increasing importance of Fano interferences when the collision velocity increases certainly cannot be accounted for by a molecular autoionization. Then it only remains a second possibility, namely, a direct coupling of the entrance channel at great R with the continuum which would provide simultaneously the excitation of the continuum and of the autoionizing states; this sudden transition cannot be considered anymore as a molecular mechanism and is identical to the atomic excitation already observed in $H^+ + He$. Certainly, in the intermediate energy range (30–100 keV), the autoionizing states are simultaneously populated by rotational coupling at $R = 0$ and by a sudden transition. In summary, the observed distortion of the angular distributions when the collision energy increases from 2.9 to 140 keV indicates an evolution of the mechanism of excitation of the autoionizing states from a quasimolecular to an atomic one.

2. Comparison of slow- and fast-particle SDCS

The SDCS compared here may be $d\sigma/d\Omega$ as well as $d\mathcal{S}/d\Omega$. To our knowledge no other data exist which compares the autoionization cross section of the fast and slow particles. Even by photon detection very little work has been done on this subject; for the He^+-He system, Wolterbeek Muller and De Heer,[48] in the energy range 0.3 to 150 keV, have found equal direct and charge-exchange excitation cross sections for some $n=3-6$ excited states of HeI (apart from antiphase oscillations in the two cross sections). Hippler *et al.*[49] compare these two cross sections between 150 and 1000 keV for the 2^1P HeI line and find different values; in a theoretical analysis of the $2^{1,3}S$ HeI excitation, Sural *et al.*[50] obtained equal direct and capture cross sections up to about 30 keV. From a comparison of the results published by Pol *et al.*[51] for the direct excitation of He ($n=2$) in the slow atom and by Gilbody *et al.*[52] for the excitation of the same levels by charge exchange in the fast atom, it also appears that a very good agreement is obtained up to 30 keV and that at 40 keV and above strong discrepancies arise [σ(exchange) > σ(direct)].

In a quasimolecular-excitation model, the He^+-He system is symmetrical because the nuclear charges are identical. The consequences of this symmetry on the SDCS measured by us can only be seen in the c.m. frame as explained in a recent letter[17]; the slow- and fast-particle excitation cross sections must be identical when referred to the same emission angle θ_{em} which is defined in Fig. 5 [see also relations (11) and (12)]. This is well verified below 15 keV [Figs. 6, 11, and 12(a)] by the cross sections measured in this work.

When the collision velocity is sufficiently high, the He^+-He system is no longer symmetrical and the excitation cross sections of the autoionizing states populated by a direct or by a charge-exchange process become different. This has been verified by Hippler *et al.*[49] for one electron 2^1P excited level of HeI; they observe an increasing disagreement between the two cross sections as the collision energy goes from 150 to 1000 keV. However, this discrepancy is the reverse [σ(direct) > σ(exchange)] of that observed from a comparison of Pol *et al.*[51] and Gilbody *et al.*[52] results below 150 keV for the total $n=2$ excitation.

In our work, the separated contributions of the ^1D and ^1P states for the fast particle are inaccurate above about 50 keV because of the very large broadening discussed in Sec. III B (see Fig. 4). This problem is eliminated when the $(^1D+^1P)$ cross sections are compared [Figs. 12(a) and 12(b)]. Our values show that discrepancies are observed between the two cross sections at 30 keV for the $(^1D+^1P)$ line especially above $\theta_{em}=90°$; this is less clear in Fig. 7 for the ^1D and ^1P lines because of greater uncertainties due to the numerical treatment. The $2s^2\,^1S$ and $2s2p\,^3P$ results are more accurate than the ^1D, ^1P ones at high energy due to the larger separation of the two lines (Fig. 4). For the $2s^2\,^1S$, smaller values are obtained in the whole angular range at 30 keV for the fast-emitter cross sections, the deviation is also greater than experimental error bar for great θ_{em} values. For example, a ratio of 1.6 is observed at $\theta_{em}=160°$. At 50 keV [Figs. 8 and 12(b)] the fast-emitter cross sections are always higher than the slow-emitter ones except in the ^1D case (but in this latter case the equality is perhaps fortuitous). At 100 and 140 keV, the discrepancies are obvious [Figs. 9, 10, and 12(b)]. All these results demonstrate that the quasimolecular-excitation model fails more and more to explain the excitation of autoionizing states above 30 keV ($v=0.55$ a.u.).

Comparing the cross sections for photon emission in various symmetrical systems as measured by different authors, Schartner *et al.*[53] conclude that the quasimolecular-excitation model is appropriate below a velocity of about 0.5 a.u. since the two cross sections are of comparable magnitude. This conclusion agrees fairly well with our own analysis but our results are certainly much more significant than those discussed by these authors; for example, it appears in Ref. 53 that the cross sections for direct and charge-exchange excitation are within a factor of 2 at about $v=0.3$ a.u. (excitation of the 3^1P HeI level). From the SDCS values discussed in this section, we may conclude that discrepancies with a molecular model are observed above $v=0.5$ a.u. (asymmetrical angular distributions and inequality of direct and charge-exchange SDCS).

V. COLLISION ENERGY DEPENDENCE OF THE CROSS SECTIONS

The energy dependence of the SDCS is shown in Fig. 13(a) at $\theta_{lab}=150°$ and 60° for the ^1D and ^1P states. It is observed that the ^1D and ^1P cross sections are almost equal and do not depend much on energy above 100 keV whatever the angle is. At lower energies, a different energy dependence is obtained for the ^1D and ^1P SDCS. The ^1P cross sections vary in the same manner independently of the angle considered. On the contrary, for the ^1D state, very different variations with collision energy are observed at 150° and 60°; as the angles around 90° have a greater influence on the total-cross-section value, it may already be conjectured that the variation observed at 60° will be recovered on the ^1D total cross section. The variation of the

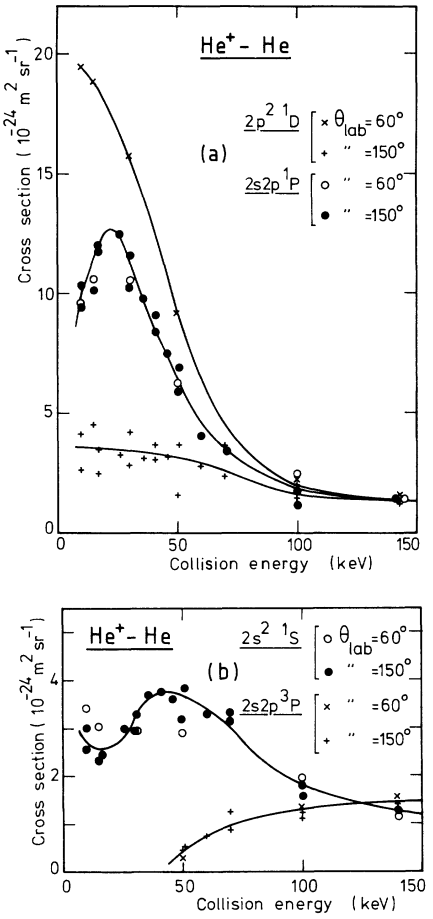

FIG. 13. Energy dependence of the single differential cross section for the excitation of the $2s^2\,{}^1S$, $2s2p\,{}^3P$, $2p^2\,{}^1D$, and $2s2p\,{}^1P$ autoionizing states. (a) $2p^2\,{}^1D$: (×) $\theta_{lab}=60°$; (+) $\theta_{lab}=150°$. $2s2p\,{}^1P$: (○) $\theta_{lab}=60°$; (●) $\theta_{lab}=150°$. (b) $2s^2\,{}^1S$: (○) $\theta_{lab}=60°$; (●) $\theta_{lab}=150°$. $2s2p\,{}^3P$: (×) $\theta_{lab}=60°$; (+) $\theta_{lab}=150°$.

^1S and ^3P cross sections is given in Fig. 13(b). As for the ^1P state, the same energy dependence is obtained at 150° and 60°. The ^1S SDCS seems to oscillate at low energy but the accuracy of our cross sections is not sufficient to be sure of this behavior. The ^3P cross-section variation is remarkable and very different from all the other ones; it is very small and not measurable below 50 keV and it increases continuously above 50 keV. It must be noted in Figs. 13(a) and 13(b) that the same value is obtained at 140 keV for the ^1S, ^3P, ^1D, and ^1P cross sections.

Total cross sections for autoionization may be considered as total *excitation* cross sections only when all the interference effects are negligible. At low-collision energy (with $E \geq 10$ keV) true excitation cross sections are measured since PCI interferences between ^1S, ^1D, and ^1P transition amplitudes do not seem to perturb the angular distribution or the line shape. For the same reason it may also be thought that Stark effect does not affect the meaning of the ^1D and ^1P total cross sections above 10 keV. Above 30 keV the angular distributions show the influence of Fano-type interferences so that, in this energy range, the measured total cross sections for the autoionizing states cannot be considered as excitation cross sections without caution. As the H^+-He data[8] clearly show that the perturbation of the angular distributions are only important for small values of θ_{lab}, we may suppose that the same thing holds for the He^+-He SDCS and hence that total cross sections are slightly affected. In the following the discussion of the behavior of these cross sections with collision energy will be made without considering further all these possible perturbations.

From Fig. 14 we may note several interesting

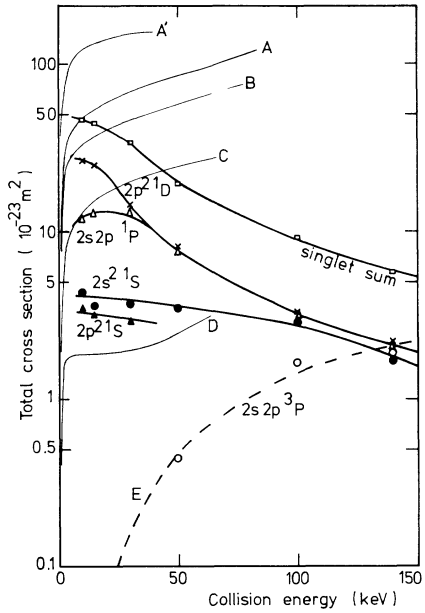

FIG. 14. Variation of the experimental total cross section for excitation of the slow particle with collision energy. The theoretical curves labeled A', A, B, C, D are taken from Koike's papers for He^{2+} on He collision; they correspond to the excitation of the following molecular states (Ref. 55) (see Fig. 15): A ($B\Sigma_g + C\Sigma_g + \Delta_g$), B ($\Delta_g$), C ($B\Sigma_g$), D ($C\Sigma_g$). Curve A' is calculated from Ref. 59 with $Z_{eff}=1.5$ as explained in the text and corresponds to the excitation of the $C\Sigma_g+\Delta_g$ molecular states. All these theoretical cross sections (Refs. 55 and 59), which give the excitation of both particles, are divided by two in order to be compared with the experimental data. Curve E gives the fit of the ^3P data with Demkov's formula $\sigma = k[1/\exp(a/v)]^{-1}$ with $k=21.6$, $a=2.7$; the collision velocity is given in atomic units.

features of the total-cross-section variations. All the autoionization total cross sections tend to the same value as the collision energy increases and the same value 2.0×10^{-23} m^2 is effectively obtained at 140 keV within only ±10%. The singlet and triplet cross sections behave in a very different way as the collision energy decreases below 140 keV. A very fast decrease is observed for the $2s2p\ ^3P$ cross section which no longer becomes measurable below 50 keV whereas the singlet cross sections increase. The ^1D and ^1P cross sections grow faster than the ^1S ones; below 30 keV the ^1D state excitation is strongly favored with respect to the ^1P one. The behavior of the singlet-states cross sections when the collision energy decreases is due to the favorable influence of the He_2^+ quasimolecule formation which gives a strong excitation of singlet states as will be explained now.

VI. DISCUSSION

In order to discuss more thoroughly the excitation sharing between the singlet states within the molecular model, it is useful to take into account the relative sublevel population values given in Table I; the total excitation cross sections for each sublevel of the $2p^2\ ^1D$ and $2s2p\ ^1P$ states are given in Table II. It appears that the $2p^2\ ^1D(2)$ (the number within the parenthesis indicates the M_L value) state excitation largely predominates that of the other channels and that the $2p^2\ ^1D$ (0) and $2p^2\ ^1S$ cross sections are rather small with respect to the former one. The possible molecular excitation mechanisms which can explain our observations will be now examined (see also Refs. 14 and 15). From the work of McCarroll and Piacentini,[46] it is well established that a double rotational coupling between the $A\Sigma_g$-$A\Pi_g$-Δ_g states (Fig. 15) at $R \approx 0$ populates the Δ_g molecular states and then the $|M_L| = 2$ atomic sublevel of the $2p^2\ ^1D$ state. However, the $C\Sigma_g$ molecular state, correlated to the same $Be^+(1s2p^2)$ united atom configuration, can also provide an excitation of the $2p^2\ ^1D(0)$ and $2p^2\ ^1S$ states[14]; the $C\Sigma_g$ state may be either directly excited by a one-step $A\Sigma_g$-$C\Sigma_g$ transition through a radial coupling[55] or by a two-step rotational coupling[54,55] $A\Sigma_g$-$A\Pi_g$-$C\Sigma_g$ at $R \approx 0$. The atomic $2s2p\ ^1P$ state must be excited by a $^2\Pi_g$ and $^2\Sigma_g$ molecular state; the results given in Table I show that the population of these two sublevels are approximatively equal. Only secondary interactions at great R with the $1s\sigma_g 2p\pi_u^2$ configurations can explain these excitations. Tentative $^2\Pi_g$ and $^2\Sigma_g$ configurations have been given in a previous paper[15] and are indicated in the schematic correlation diagram (Fig. 15). A similar secondary interaction explains the $2p^2\ ^1D(1)$ sublevel excitation. The

TABLE II. Total cross sections for the various autoionizing states in He^+ on He collisions. All the values are given in 10^{-23} m^2 units; they have been obtained by a fit of the experimental values by relations (7′) or (10) (see text). This explains small discrepancies between the values given for $(2p^2\ ^1D + 2s2p\ ^1P)$ and the $2p^2\ ^1D$ and $2s2p\ ^1P$ sum of the separated contributions. The labels F and S mean that the fast- and slow-particle excitation are considered.

Collision energy (keV)		10	15	30	50	100	140
$2s^2\ ^1S$	S	4.4	3.6	3.7	3.5	2.9	1.7
	F	4.6	3.6	3.1			
$2s2p\ ^3P$	S				0.45	1.7	1.9
$2p^2\ ^1D\ \|M_L\| = 2$	S	24.6	22.2				
	F	21.2	19.4				
$\|M_L\| = 1$	S	0.8	0.7				
	F	2.7	1.8				
$\|M_L\| = 0$	S	0.8	1.7				
	F	1.0	1.1				
total	S	26.2	24.6	14.5	8.1	3.3	2.2
	F	24.9	22.3				
$2s2p\ ^1P\ \|M_L\| = 1$	S	7.1	8.4				
	F	6.5	8.2				
$\|M_L\| = 0$	S	4.6	4.3				
	F	4.7	4.6				
total	S	11.7	12.6	13.0	7.6	3.2	2.0
	F	11.2	12.8				
$2p^2\ ^1D + 2s2p\ ^1P$	S	36.7	34.0	27.5	15.6	6.5	4.3
	F	36.7	34.3	25.8	18.8		
$2p^2\ ^1S$	S	3.5	3.2	2.9			
sum of the measured singlet cross sections	S	45.8	44.1	34.1	19.2	9.4	5.9

$2s^2\ ^1S$ state excitation can take place through various mechanisms: The $A\Sigma_g$-$B\Sigma_g$ radial coupling is weak in our energy range.[54,55] Koike *et al.*[55] have shown that a rotational coupling between the $A\Pi_g$ and $B\Sigma_g$ states is much more efficient to excite the $B\Sigma_g$ molecular state and hence the $2s^2\ ^1S$ atomic state. As the various possible couplings do not affect the spin direction of the two $2p\sigma_u$ electrons which are opposite in the $A\Sigma_g$ state, the promotion of these $2p\sigma_u$ electrons cannot give rise to the excitation of a triplet diexcited state like the $2s2p\ ^3P$ one. The absence of the $2s2p\ ^3P$ line in our spectra below 30 keV is then in good agreement with the molecular model.

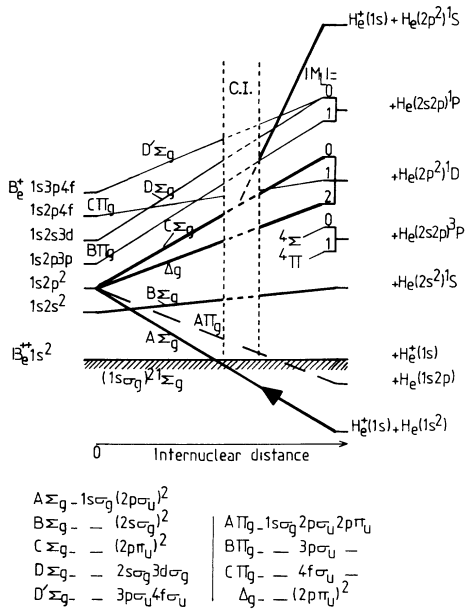

FIG. 15. Schematic diabatic correlation diagram for the energy states of the He^++ He system. The configuration interactions (CI) which mix the various states at great internuclear distances prevent us from making a one to one correspondence between the known molecular states at small R and the atomic autoionizing states as $R \to \infty$.

Considering only the ^1D excitation, Kessel *et al.*[38] suggest that the primary rotational coupling at small R can provide an excitation of all the sublevels $M_L = 0, 1, 2$ of the ^1D state. Their interpretation relies on the application of the model of Eriksen *et al.*,[56,57] initially developed for a primary radial coupling, to the rotational coupling at small R. It seems that this model which was very convincing in the case of a radial coupling becomes much more doubtful when applied to the rotational coupling. For example, it obliges Kessel *et al.* to assume that only a Σ_g state is initially excited by the rotational coupling (this is the $C\Sigma_g$ state as identified in Ref. 39). All the theoretical works[46,54,55,58] generally admit that, on the contrary, the Δ_g excitation is preponderant. This is particularly clear in Ref. 55 where it is shown that the excitation coming from the $C\Sigma_g$ state is by far smaller than the one coming from the Δ_g state. Moreover, these theoretical results are rather convincing since they compare well with our own experimental findings as will be shown below. Therefore the interpretation of Kessel *et al.*[38] will not be considered further in the following.

We may now attempt to understand the relative total-cross-section values we obtain. The only detailed quantitative theoretical work on the two-electron excitation in a symmetrical system has been done by Koike *et al.*[55] for He^{2+} on He, in the 0.5–50 keV energy range. Their total cross sections for the excitation of the Δ_g, $B\Sigma_g$, and $C\Sigma_g$ molecular states are given in Fig. 14; the values have been divided by two in order to make the comparison with our slow particle excitation cross section σ_s valuable (it is assumed that $\sigma_s = \sigma_f$). It is worth noting also that the theoretical cross sections correspond to the excitation of a molecular state which dissociates at infinite R into $He^{2+} + He(2p^2)$ as well as $He^+(2p) + He^+(2p)$; since the branching ratio between these two channels remains unknown we must be careful when we compare our data with these theoretical values. Moreover, the He^+-He and He^{2+}-He systems differ by one $1s\sigma_g$ electron; then, we may infer that the screening effect of the third electron cannot be neglected. Its influence on the cross-section value is illustrated with the use of the scaled cross section for the excitation of the $(2p\pi_u^2\Delta_g + 2p\pi_u^2\Sigma_g)$ molecular state given by these authors in a recent paper[59] (the scaling parameter is the effective nuclear charge Z_{eff}). If we suppose that the screened nuclear charge of the $[Be^{4+} + e^-(1s)]$ united atom as seen by the $2p$ electrons is equal to the limit value three, then we can take $Z_{\text{eff}} = 1.5$ and calculate the new cross section [Eq. (25) in Ref. 59] (curve A′ in Fig. 14). We see that the absolute value of the cross section is strongly dependent on Z_{eff}. The comparison of the relative initial population of the $C\Sigma_g$ and Δ_g molecular states as given by the theory[55] with the observed relative excitation of the autoionization channels at great R is not straightforward. The molecular $C\Sigma_g$ and Δ_g states dissociate at infinite R into several channels: autoionization of one particle, simultaneous one-electron excitation of both particles, and, in the He^+ on He system, excitation of a negative resonance $[He^{2+} + He^-(1s2p^2)]$. The latter one is supposed to be negligible since no line corresponding to the decay of this autoionizing negative resonance was ever observed in our spectra. Then as the branching ratio (autoionization and simultaneous excitation) is the same for the dissociation of the $C\Sigma_g$ and Δ_g states, we can assume that the same relative population must be observed between the autoionizing dissociation channels $[2p^2\,^1D(0) + 2p^2\,^1S]$ and $2p^2\,^1D(2)$ provided that the various configuration interactions at great R, which explain the $2p^2\,^1D$ and $2s2p\,^1P$ states excitation, do not destroy completely this population ratio. Nevertheless, the calculations of Koike *et al.*[55] show the influence of various molecular excitation mechanisms on the atomic autoionizing state excitations. Remarkable similarities are observed between our data at 10–

15 keV and the theoretical results:

(1) The strong observed excitation of the $2p^2\,{}^1D(2)$ state shows that the two step $A\Sigma_g$-$A\Pi_g$-Δ_g rotational coupling is preponderant in He^+ on He as it is in He^{2+} on He.

(2) In the two cases, the $[2p^2\,{}^1D(0)+2p^2\,{}^1S]$ excitation is much smaller than the $2p^2\,{}^1D(2)$ one. As shown in the He^{2+} on He case,[55] this indicates that the radial coupling $A\Sigma_g$-$C\Sigma_g$, which mainly contributes to the $C\Sigma_g$ excitation, is less efficient than the rotational coupling $A\Pi_g$-Δ_g. The rotational coupling $A\Pi_g$-$C\Sigma_g$ only contributes for a small part since Koike *et al.* have shown that it is zero at $R=0$ and that it remains much smaller than the $A\Pi_g$-Δ_g coupling for higher R values.

(3) For the two systems the $2s^2\,{}^1S$ excitation is smaller than the $2p^2\,{}^1D(2)$ one but we obtain about the same values for the $2s^2\,{}^1S$ and $[2p^2\,{}^1D(0)+2p^2\,{}^1S]$ cross sections whereas the theoretical results indicate a ratio of 10 between the $B\Sigma_g$ and $C\Sigma_g$ cross sections.

On the whole, the agreement between the theoretical results, which describe the excitation of the molecular states at small R values, and our results, which give the remaining excitation at infinite R on the atomic autoionization channels, indicate that the secondary interactions at great R do not completely destroy the initial relative populations of the molecular states. It is worth noting that Koike's results disagree with some conclusions of Gauyacq[54] for the neutral He on He system. Following this author the $A\Pi_g$-$C\Sigma_g$ and $A\Pi_g$-Δ_g rotational couplings would be equal at $R=0$; moreover, the direct coupling $A\Sigma_g$-$C\Sigma_g$ would be negligible. Of course, our results can no longer be understood in a straightforward manner if we suppose that the initial populations of the Δ_g and $C\Sigma_g$ molecular states are equal; the much smaller value of the $[2p^2\,{}^1S+2p^2\,{}^1D(0)]$ cross section with respect to the $2p^2\,{}^1D(2)$ one would then be ascribed to a greater depopulation of the $C\Sigma_g$ channel at great R.

As the excitation of the $2p^2\,{}^1D(0)$ and $2p^2\,{}^1S$ states comes from the same $C\Sigma_g$ molecular state, it is interesting to compare the corresponding cross-section values. A correct description of the excitation of these two states is only made when a mixing between the $1s\sigma_g 2p\pi_u^2$ and $1s\sigma_g 4f\sigma_u^2$ configurations is made (a similar discussion can be found in Ref. 60 in the case Na^+-Ne). It may be shown that the excitation amplitudes for the two atomic channels due to the $C\Sigma_g$ state are given by[61]

$$\begin{pmatrix} 1s\sigma_g 2p\pi_u^2\,{}^2\Sigma_g \\ 1s\sigma_g 4f\sigma_u^2\,{}^2\Sigma_g \end{pmatrix} = \frac{1}{\sqrt{3}} \begin{pmatrix} \sqrt{2} & 1 \\ -1 & \sqrt{2} \end{pmatrix} \begin{pmatrix} 2p^2\,{}^1D(0) \\ 2p^2\,{}^1S \end{pmatrix}.$$

At low collision velocity v, only the lowest $2p^2\,{}^1D(0)$ state is excited whereas at the limit $v\to\infty$, we should have

$$\frac{\sigma(2p^2\,{}^1S)}{\sigma(2p^2\,{}^1D(0))} \xrightarrow[v\to\infty]{} 2,$$

which is a maximum value for this ratio. Before comparing with experiment, we must note that the $2p^2\,{}^1D(0)$ cross sections are certainly subject to large error bars since they are a factor 3 smaller than the $2s2p\,{}^1P(0)$ one. The differences between the four values given at 10–15 keV (Table II) are not significant and only a mean value 2.2×10^{-23} m^2 must be taken. The experimental ratio at 10–15 keV is then $\sigma(2p^2\,{}^1S)/\sigma(2p^2\,{}^1D(0))=2.9$. This too high value is understood by considering first that configuration interaction at great R depopulates the two molecular states and secondly that the $2p^2\,{}^1D(0)$ channel is more depopulated than the $2p^2\,{}^1S$ one.

Concerning the energy dependence of the singlet cross sections with collision energy, we observe that the $E^{1/3}$ variation expected for one electron[62] $2p\sigma_u \to 2p\pi_u$ or two electron $2p\sigma_u^2 \to 2p\sigma_u 2p\pi_u \to 2p\pi_u^2$ excitation through a rotational coupling is not observed above 10 keV (this variation is almost given by curve A in Fig. 14). This shows that the molecular model cannot alone explain the excitation of these singlet autoionizing states above 10–15 keV.

Let us consider now the remarkable behavior of the $2s2p\,{}^3P$ cross section (Fig. 14) which increases quickly with the collision energy. As mentioned earlier the excitation of such a triplet state is unlikely to occur within the molecular model. The nonobservation of this line below 50 keV is a supplementary indication that the molecular model works well in this energy range. On the other hand the ^3P excitation points out that above 50 keV part of the autoionizing state excitation is due to sudden transitions from the entrance channel to the continuum. This is a new confirmation of our previous interpretation that the asymmetrical angular distributions and the inequality of direct and charge-exchange SDCS observed above 0.55 a.u. are due to atomic-type sudden transitions to the continuum. Considering the collision-velocity dependence of this cross section it is shown in Fig. 14 that it varies as $k[1+\exp(a/v)]^{-1}$, where a and k are two velocity independent parameters determined by a fitting procedure: $k=21.6$, $a=2.7$ when v is expressed in atomic units. It must be noted that this behavior looks like the exponential law given by the Demkov-Meyerhof model which was shown to be applicable to a transition to the continuum by Rudd.[63] That the ^3P cross section equals the singlet ones at 140 keV is also another consequence of the very weak influence of the

molecular model on the excitation of the autoionizing states at this energy.

VII. COMPARISON OF THE He^+-He AND H^+-He SYSTEMS

In order to seek for the influence of the collision partners in the excitation of the helium autoionizing states, we compare in Fig. 16 our present results with total cross sections deduced from $d\$/d\Omega$ values obtained in H^+ on He collisions.[8,25] The integration of these angular distributions is certainly very inaccurate in the small-angle range since very important oscillations were observed which precluded a fit of these curves with a relation such as (10). So, for proton data, we have attempted to integrate the angular distributions by a numerical method using extrapolated values at 10°; these values take into account that the ratio of Shore parameters (b/a) is known from the Fano $\tilde{q}$ parameter value measured at 10°. At $\theta_{lab}=0°$, b was taken as zero; in the backward direction we considered that the cross section remains constant above $\theta_{lab}=160°$. With such precautions, we did not observe variations greater than ±10% on the total cross section values when we take various extrapolated values at 10°. The ^1D and ^1P values are much more inaccurate than the ^1S one because of the greater uncertainties on the corresponding $d\$/d\Omega$ values.[8] The results are given in Fig. 16. From the $d\$(^1S)/d\Omega$ variation obtained at $\theta_{lab}=157°$ in Ref. 8, we may guess that the ^1S total cross section decreases below $v=0.9$–1.1 a.u. (20–30 keV) as the ^1D and ^1P cross section do below 1.7 a.u. These variations at low energy are due to the negative influence of the quasimolecule HHe^+ formation which, contrary to the He_2^+ case, makes inelastic processes very unlikely to occur due to a large energy gap between the $1s\sigma^2\Sigma$ entrance channel and the $1s\sigma 2p\sigma\Sigma$ promoted state.

Comparing now H^+ and He^+ results, we observe that, by a smooth extrapolation of He^+ data towards higher velocities, about the same cross sections are obtained (within perhaps a factor of 2) above $v\approx 1.5$ a.u. The $2\,^1P$ HeI level excitation by H^+ and He^+ impact was investigated by Moiseiwitsch and Stewart[64] using Born's approximation. They also found similar values for the two cross sections above $v\approx 1$ a.u. Then it appears that the He^+ particle behaves as a unit-charge nucleus at sufficiently high velocity for the singlet-state excitation. However, the different line-shape parameters $\tilde{q}$ (Sec. III A) found at $v\approx 1.2$ a.u. are in disagreement with this conclusion.

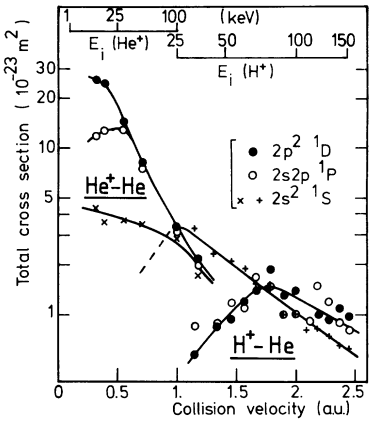

FIG. 16. Comparison of the total cross sections for autoionization of the $2s^2\,^1S$, $2p^2\,^1D$, and $2s2p\,^1P$ states as measured in He^+ on He and H^+ on He collisions.

The results given in Fig. 16 also show another remarkable similarity of the two systems. We note that above 70 keV for the H^+ on He collision ($v\approx 1.7$ a.u.) and 100 keV ($v=1$ a.u.) for the He^+ on He system, the cross section becomes independent of the angular momentum; this result is also in disagreement with a quasimolecular-excitation mechanism which often favors some line excitation.

VIII. CONCLUSION

We have studied in this paper the influence of the quasimolecule formation on the excitation of helium atomic autoionizing states. Above a velocity of about $v=0.5$ a.u., direct coupling with the continuum competes with the electron promotion mechanism. As a consequence, interferences between direct resonant and nonresonant transition amplitudes perturb the angular distribution and the line shapes; the direct and charge-exchange SDCS and total cross sections take different values. The excitation of the $2s2p\,^3P$ state above $v=0.7$ a.u. also gives evidence that departure from the quasimolecular model becomes important in this velocity range. The comparison of H^+ and He^+ impact data shows that the same cross sections are obtained above $v\approx 1.5$ a.u. for the two systems. Moreover, it seems that the cross section value becomes independent of the autoionizing state considered above $v\approx 1.2$ a.u. in He^+ on He and $v\approx 1.7$ a.u. in H^+ on He; all these results also give an upper limit of validity of the quasimolecule model.

[1]U. Fano, Phys. Rev. 124, 1866 (1961).
[2]V. V. Balashov, S. S. Lipovetsky, and V. S. Senashenko, Zh. Eksp. Teor. Fiz. 63, 1622 (1972) [Sov. Phys.—JETP 36, 858 (1973)].
[3]A. Bordenave-Montesquieu and P. Benoit-Cattin, C. R. Acad. Sci. 272, 1473 (1971); Phys. Lett. 36A, 243 (1971).
[4]N. Stolterfoht, Phys. Lett. 37A, 117 (1971).
[5]N. Stolterfoht, D. Ridder, and P. Ziem, Phys. Lett. 42A, 240 (1972); D. Ridder, N. Stolterfoht, and P. Ziem, *Proceedings of the Eighth International Conference on the Physics of Electronic and Atomic Collisions, Belgrade, 1973,* edited by B. C. Čobić and M. V. Kurepa (Institute of Physics, Belgrade, 1973).
[6]F. D. Schowengerdt and M. E. Rudd, Phys. Rev. Lett. 28, 127 (1972).
[7]A. Bordenave-Montesquieu, A. Gleizes, M. Rodiere, and P. Benoit-Cattin, J. Phys. B 6, 1977 (1973); A. Bordenave-Montesquieu, P. Benoit-Cattin, M. Rodiere, and A. Gleizes, *Proceedings of the Eighth International Conference on the Physics of Electronic and Atomic Collisions, Belgrade, 1973,* edited by B. C. Čobić and M. V. Kurepa (Institute of Physics, Belgrade, 1973).
[8]A. Bordenave-Montesquieu, Ph.D. thesis, Université P. Sabatier, Toulouse, 1973 (unpublished) (available from the CNRS: AO-CNRS-10089); A. Bordenave-Montesquieu, P. Benoit-Cattin, M. Rodiere, A. Gleizes, and H. Merchez, J. Phys. B 8, 874 (1975).
[9]S. S. Lipovetsky and V. S. Senashenko, J. Phys. B 5, L183 (1972); *Proceedings of the Eighth International Conference on the Physics of Electronic and Atomic Collisions, Belgrade, 1973,* edited by B. C. Čorbić and M. V. Kurepa (Institute of Physics, Belgrade, 1973); J. Phys. B 7, 693 (1974).
[10]M. Prost, R. Morgenstern, D. Schneider, and N. Stolterfoht, *Abstract of the Tenth International Conference on the Physics of Electronic and Atomic Collisions, Paris, 1977,* edited by M. Barat and J. Reinhardt (Commissariat à l'Energie Atomique, Paris, 1977); M. Prost, diplomarbeit, Freien Universitat Berlin, 1978 (unpublished).
[11]M. E. Rudd and J. H. Macek, Case Stud. At. Phys. 3, 47 (1972).
[12]F. D. Schowengerdt, S. R. Smart, and M. E. Rudd, Phys. Rev. A 7, 560 (1973).
[13]B. Cleff and W. Mehlhorn, J. Phys. B 7, 593 (1974).
[14]A. Bordenave-Montesquieu, P. Benoit-Cattin, A. Gleizes, and H. Merchez, J. Phys. B 8, L350 (1975).
[15]A. Bordenave-Montesquieu, P. Benoit-Cattin, M. Boudjema, and A. Gleizes, *Abstract of the Tenth International Conference on the Physics of Electronic and Atomic Collisions, Paris, 1977,* edited by M. Barat and J. Reinhardt (Commissariat à l'Energie Atomique, Paris, 1977).
[16]R. Morgenstern, A. Niehaus, and U. Thielmann, Phys. Rev. Lett. 37, 199 (1976); R. Morgenstern, A. Niehaus, and U. Thielmann, J. Phys. B 10, 1039 (1977); R. Morgenstern and A. Niehaus, in *Coherence and Correlation in Atomic Collisions*, edited by H. Kleinpoppen and J. F. Williams (Plenum, New York, 1980), p. 229.
[17]A. Gleizes, A. Bordenave-Montesquieu, and P. Benoit-Cattin, J. Phys. B 13, L577 (1980).
[18]R. B. Barker and H. W. Berry, Phys. Rev. 151, 14 (1966); H. W. Berry, *ibid.* 127, 1634 (1962).
[19]A. Gleizes, P. Benoit-Cattin, A. Bordenave-Montesquieu, and H. Merchez, J. Phys. B 9, 473 (1976).
[20]N. Stolterfoht, D. Brandt, and M. Prost, Phys. Rev. Lett. 43, 1654 (1979); *Proceedings of the Eleventh International Conference on the Physics of Electronic and Atomic Collisions, Kyoto, 1979,* edited by K. Takayanagi and N. Oda (North-Holland, Amsterdam, 1979).
[21]D. Brandt, M. Prost, and N. Stolterfoht, *Proceedings of the Eleventh International Conference on the Physics of Electronic and Atomic Collisions, Kyoto, 1979,* edited by K. Takayanagi and N. Oda (North-Holland, Amsterdam, 1979).
[22]P. Benoit-Cattin, D. Blanc, A. Bordenave-Montesquieu, A. Gleizes, M. Rodiere, and S. Sobhanian, J. Phys. E 6, 564 (1973).
[23]M. E. Rudd and T. Jorgensen, Phys. Rev. 131, 666 (1963).
[24]M. E. Rudd, L. H. Toburen, and N. Stolterfoht, At. Data Nucl. Data Tables 18, 413 (1976).
[25]A. Bordenave-Montesquieu, P. Benoit-Cattin, A. Gleizes, and H. Merchez, At. Data Nucl. Data Tables 17, 157 (1976).
[26]M. E. Rudd, C. A. Sautter, and C. L. Bailey, Phys. Rev. 151, 20 (1966); M. E. Rudd and D. H. Madison, Phys. Rev. A 14, 128 (1976).
[27]J. Slevin, M. Eminyan, and K. B. McAdam, J. Phys. E 8, 1000 (1975).
[28]P. L. Altick and E. N. Moore, Phys. Rev. 147, 59 (1966); A. K. Bhatia and A. Temkin, *ibid.* 182, 15 (1969); A. K. Bhatia, P. G. Burke, and A. Temkin, Phys. Rev. A 8, 21 (1973); A. K. Bhatia and A. Temkin, *ibid.* 11, 2018 (1975); P. G. Burke and D. D. McVicar, Proc. Phys. Soc. London 86, 989 (1965); P. G. Burke and A. J. Taylor, *ibid.* 88, 549 (1966); P. G. Burke, Ad. At. Mol. Phys. 4, 173 (1968); J. W. Cooper, S. Ormonde, C. H. Humphrey, and P. G. Burke, Proc. Phys. Soc. London 91, 285 (1967); P. J. Hicks and J. Comer, J. Phys. B 8, 1866 (1975); R. P. Madden and K. Codling, Astrophys. J. 141, 964 (1965); W. Miller, Phys. Rev. 152, 70 (1966); R. H. Perrott and A. L. Stewart, J. Phys. B 1, 381 (1968); R. H. Perrott and A. L. Stewart, *ibid.* 1, 1226 (1968); D. E. Ramaker and D. M. Schrader, J. Chem. Phys. 55, 471 (1971).
[29]V. N. Ostrovskii, Zh. Eksp. Teor. Fiz. 72, 2079 (1977) [Sov. Phys.—JETP 45, 1092 (1977)].
[30]A. Z. Devdariani, V. N. Ostrovskii, and Yu. N. Sebyakin, Zh. Eksp. Teor. Fiz. 73, 412 (1977) [Sov. Phys.—JETP 46, 215 (1977)].
[31]R. J. Tweed, J. Phys. B 9, 1725 (1976).
[32]F. H. Read and J. Comer, in *Coherence and Correlation in Atomic Collisions*, edited by H. Kleinpoppen and J. F. Williams (Plenum, New York, 1980), p. 243.
[33]J. S. Risley, A. K. Edwards, and R. Geballe, Phys. Rev. A 9, 1115 (1974).
[34]N. Stolterfoht, D. Schneider, D. Burch, B. Aagaard, E. Boving, and B. Fastrup, Phys. Rev. A 12, 1313 (1975).
[35]P. Dahl, M. Rodbro, B. Fastrup, and M. E. Rudd, J. Phys. B 9, 1567 (1976).
[36]R. G. Sachs, *Nuclear Theory* (Addison-Wesley, Reading, Massachusetts, 1955), Chap. 10.
[37]U. Fano and J. H. Macek, Rev. Mod. Phys. 45, 553 (1973).

[38]Q. C. Kessel, R. Morgenstern, B. Muller, and A. Niehaus, Phys. Rev. A 20, 804 (1979); Q. C. Kessel, R. Morgenstern, B. Muller, A. Niehaus, and U. Thielmann, Phys. Rev. Lett. 40, 645 (1978).
[39]R. Morgenstern, *Invited Papers and Progress Reports from the Eleventh International Conference on the Physics of Electronic and Atomic Collisions, Kyoto, 1979*, edited by K. Takayanagi and N. Oda (North-Holland, Amsterdam, 1979).
[40]D. Bordenave-Montesquieu and R. Dagnac, J. Phys. B 12, 1233 (1979).
[41]D. Bordenave-Montesquieu, thèse de doctorat d'Etat, Université Paul Sabatier, Toulouse, 1980 (unpublished).
[42]A. Bordenave-Montesquieu, A. Gleizes, P. Benoit-Cattin, and M. Boudjema, J. Phys. E 13, 209 (1980).
[43]A. Gleizes, thèse de doctorat d'Etat No. 962, Université Paul Sabatier, Toulouse, 1980 (unpublished).
[44]W. Shearer-Izumi, At. Data Nucl. Data Tables 20, 531 (1977).
[45]J. S. Risley and R. Geballe, Phys. Rev. A 10, 2206 (1974).
[46]R. McCarroll and R. D. Piacentini, J. Phys. B 4, 1026 (1971); R. McCarroll, *Invited Papers and Progress Reports from the Eighth International Conference on the Physics of Electronic and Atomic Collisions, Belgrade, 1973*, edited by B. C. Čobić and M. V. Kurepa (Institute of Physics, Belgrade, 1973), p. 72.
[47]V. Sidis, J. Phys. B 6, 1188 (1973).
[48]L. Wolterbeek Muller and F. J. De Heer, Physica (Utrecht) 48, 345 (1970).
[49]R. Hippler, K. H. Schartner, and H. F. Beyer, J. Phys. B 11, L337 (1978).
[50]D. P. Sural, S. C. Mukherjee, and N. C. Sil, Phys. Rev. 164, 156 (1967).
[51]V. Pol, W. Kauppila, and J. T. Park, Phys. Rev. A 8, 2990 (1973).
[52]H. B. Gilbody, K. F. Dunn, R. Browning, and C. J. Latimer, J. Phys. B 4, 800 (1971).
[53]K. H. Schartner, R. Hippler, and H. F. Beyer, J. Phys. B 10, 93 (1977).
[54]J. P. Gauyacq, J. Phys. B 9, 2289 (1976).
[55]F. Koike, H. Nakamura, S. Hara, Y. Itikawa, M. Matsuzawa, H. Sato, and I. Shimamura, J. Phys. B 11, 4193 (1978).
[56]F. J. Eriksen, D. H. Jaecks, W. De Rijk, and J. Macek, Phys. Rev. A 14, 119 (1976).
[57]J. Macek, Seventh International Conference on Ion-Atom Collisions, Tokai-Ibaraki, Japan, 1979 (unpublished).
[58]B. Stern, J. P. Gauyacq, and V. Sidis, J. Phys. B 11, 653 (1978).
[59]F. Koike, M. Matsuzawa, S. Hara, Y. Itikawa, H. Nakamura, H. Sato, and I. Shimamura, J. Phys. B 12, 2325 (1979).
[60]J. Ostgaard Olsen, T. Andersen, M. Barat, Ch. Courbin-Gaussorgues, V. Sidis, J. Pommier, J. Agusti, N. Andersen, and A. Russek, Phys. Rev. A 19, 1457 (1979).
[61]V. Sidis, Ecole d'été de Physique de Toulouse, 1978 (unpublished).
[62]J. S. Briggs, Rep. Prog. Phys. 39, 217 (1976).
[63]M. E. Rudd, Phys. Rev. A 20, 787 (1979).
[64]B. L. Moiseiwitsch and A. L. Stewart, Proc. Phys. Soc. London 67, 1069 (1954).